

Long-term trends in urban NO₂ concentrations and associated pediatric asthma cases: estimates from global datasets

Susan Anenberg^{1,1}, Arash Mohegh^{1,1}, Daniel L. Goldberg^{2,2}, Michael Brauer^{3,3}, Katrin Burkart^{4,4}, Perry Hystad^{5,5}, Andrew Larkin^{5,5}, and Sarah Wozniak^{4,4}

¹George Washington University

²George Washington University, Argonne National Laboratory

³University of British Columbia, Institute for Health Metrics and Evaluation

⁴Institute for Health Metrics and Evaluation

⁵Oregon State University

November 30, 2022

Abstract

Background: Combustion-related nitrogen dioxide (NO₂) air pollution is associated with pediatric asthma incidence. We estimated global surface NO₂ concentrations consistent with the Global Burden of Disease Study for 1990-2019 at 1km resolution, and concentrations and attributable pediatric asthma incidence trends in 13,189 cities from 2000-2019. Methods: We scaled an existing surface annual average NO₂ concentrations dataset for 2010-2012 from a land use regression model (based on 5,220 NO₂ monitors in 58 countries and land use variables) to other years using NO₂ column densities from satellite and reanalysis datasets. We applied these concentrations to epidemiologically-derived concentration-response factors, population, and baseline asthma rates to estimate NO₂-attributable pediatric asthma incidence. Findings: We estimated that 1.85 million (95% uncertainty interval: 0.93 – 2.8 million) new pediatric asthma cases were attributable to NO₂ globally in 2019, two-thirds of which occurred in urban areas. The fraction of pediatric asthma incidence that is attributable to NO₂ in urban areas declined from 20% in 2000 to 16% in 2019. Urban attributable fractions dropped in High-income (-41%), Latin America/Caribbean (-16%), Central Europe, Eastern Europe, and Central Asia (-13%), and Southeast Asia, East Asia, and Oceania (-6%), and rose in South Asia (+23%), Sub-Saharan Africa (+11%), and North Africa and Middle East (+5%) regions. The importance of NO₂ concentrations, pediatric population size, and asthma incidence rates in driving these changes differs regionally. Interpretation: Despite improvements in some regions, combustion-related NO₂ pollution continues to be an important contributor to pediatric asthma incidence globally, particularly in cities. Funding: Health Effects Institute, NASA

1 **Long-term trends in urban NO₂ concentrations and associated pediatric asthma incidence: estimates**
2 **from global datasets**

3
4 Susan C. Anenberg^{1*}, Arash Mohegh^{1*}, Daniel L. Goldberg^{1,2}, Gaige H. Kerr¹, Michael
5 Brauer^{3,4}, Katrin Burkart³, Perry Hystad⁵, Andrew Larkin⁵, Sarah Wozniak³, Lok Lamsal⁶

6 1 Milken Institute School of Public Health, George Washington University, Washington, DC,
7 USA

8 2 Energy Systems Division, Argonne National Laboratory, Washington, DC, USA

9 3 Institute for Health Metrics and Evaluation, University of Washington, Seattle, Washington,
10 USA

11 4 University of British Columbia, Vancouver, BC, Canada

12 5 Oregon State University, Corvallis, OR, USA

13 6 NASA Goddard Space Flight Center, Greenbelt, MD, USA

14 * These authors contributed equally to this work.

15 Corresponding author: Susan Anenberg, 950 New Hampshire Ave NW, Washington, DC 20052,
16 sanenberg@gwu.edu, 1-202-994-2392

17

18 **Abstract**

19 **Background:** Combustion-related nitrogen dioxide (NO₂) air pollution is associated with
20 pediatric asthma incidence. We estimated global surface NO₂ concentrations consistent with the
21 Global Burden of Disease Study for 1990-2019 at 1km resolution, and concentrations and
22 attributable pediatric asthma incidence trends in 13,189 cities from 2000-2019.

23 **Methods:** We scaled an existing surface annual average NO₂ concentrations dataset for 2010-
24 2012 from a land use regression model (based on 5,220 NO₂ monitors in 58 countries and land
25 use variables) to other years using NO₂ column densities from satellite and reanalysis datasets.
26 We applied these concentrations to epidemiologically-derived concentration-response factors,
27 population, and baseline asthma rates to estimate NO₂-attributable pediatric asthma incidence.

28 **Findings:** We estimated that 1.85 million (95% uncertainty interval: 0.93 – 2.8 million) new
29 pediatric asthma cases were attributable to NO₂ globally in 2019, two-thirds of which occurred in
30 urban areas. The fraction of pediatric asthma incidence that is attributable to NO₂ in urban areas
31 declined from 20% in 2000 to 16% in 2019. Urban attributable fractions dropped in High-income
32 (-41%), Latin America/Caribbean (-16%), Central Europe, Eastern Europe, and Central Asia (-
33 13%), and Southeast Asia, East Asia, and Oceania (-6%), and rose in South Asia (+23%), Sub-
34 Saharan Africa (+11%), and North Africa and Middle East (+5%) regions. The importance of
35 NO₂ concentrations, pediatric population size, and asthma incidence rates in driving these
36 changes differs regionally.

37 **Interpretation:** Despite improvements in some regions, combustion-related NO₂ pollution
38 continues to be an important contributor to pediatric asthma incidence globally, particularly in
39 cities.

40 **Funding:** Health Effects Institute, NASA

41

42 **Research in context:**

43 **Evidence before this study:** We searched PubMed and Google Scholar databases for studies
44 published in English from the database inception until March 11, 2021, using the search terms
45 (“NO₂” OR “nitrogen dioxide”) AND “asthma” AND “trends”. Previous studies have reported
46 epidemiological analyses linking changes with asthma to changes in NO₂, or have assessed long-
47 term trends in NO₂ concentrations in some countries or world regions. However, these studies
48 provide little information about how NO₂ concentrations are changing in urban areas all around
49 the world, and the influence those changes have on pediatric asthma incidence. An earlier study
50 published in 2019 showed that over 4 million new pediatric asthma cases, representing ~13% of
51 all pediatric asthma incidence worldwide in 2015, could be attributed to NO₂ pollution.

52 Understanding temporal trends in NO₂-attributable pediatric asthma incidence could help inform
53 asthma and air pollution mitigation strategies.

54 **Added value of this study:** We show that urban areas experience higher NO₂ concentrations and
55 disease burdens compared with rural areas, with 16% of pediatric asthma incidence in urban
56 areas estimated to be attributable to NO₂ pollution. We also find that the fraction of pediatric
57 asthma incidence that is attributable to NO₂ declined in High-income, Latin American and
58 Caribbean, Central Europe, Eastern Europe, and Central Asia from 2000 to 2019, and increased
59 in the rest of the world, particularly in South Asia and Sub-Saharan Africa. In carrying out this
60 work, we produced the most spatially resolved (1km x 1km) long-term (1990-2019) dataset of
61 surface NO₂ concentrations, which is compatible with the Global Burden of Disease Study and is
62 now publicly available. Our study also demonstrates the utility of satellite remote sensing for
63 environmental and public health surveillance in urban areas worldwide.

64 **Implications of all the available evidence:** Current levels of NO₂ contribute substantially to
65 pediatric asthma incidence, particularly in cities. Mitigating air pollution should be a critical
66 element of children’s public health strategies.

67 **Acknowledgements:** This work was supported by grants from the Health Effects
68 Institute/Bloomberg Philanthropies (Research Agreement #4977/20-11) and NASA (Grant
69 #80NSSC19K0193). We gratefully acknowledge the developers of the OMI NO₂ concentration
70 products, GHS-SMOD urban area dataset, GBD disease rate datasets, and Worldpop population
71 dataset. We appreciate helpful discussions with Bryan Duncan. The contents of this article do not
72 necessarily reflect the views of HEI, or its sponsors.

73 **Data availability:** NO₂ concentrations are available at:

74 https://figshare.com/articles/dataset/Global_surface_NO2_concentrations_1990-2020/12968114.

75 Estimated NO₂-attributable asthma incidence results are available at:
76 https://github.com/AMohegh/Asthma_NO2_urban

77 **Author contributions:** SCA, AM, and DG designed the study; PH, AL, and LL provided data;
78 AM and GK carried out the calculations, SCA, AM, DG, MB, PH, AL, and SW contributed
79 input on methods development; SCA and AM wrote the paper; all authors helped interpret results
80 and reviewed the manuscript. AM, GK, and DG have verified the underlying data.

81 **Declaration of interests:** The authors declare no conflict of interest.

82
83 **Introduction**

84 Nitrogen dioxide (NO₂), a component of nitrogen oxides (NO_x), is a pervasive air pollutant that
85 is a precursor for ground-level ozone and fine particulate matter (PM_{2.5}), the leading contributors
86 to air pollution-related mortality.¹ Major anthropogenic NO₂ sources include on-road and non-
87 road transportation tailpipe emissions (including heavy-, medium-, and light-duty vehicles,
88 shipping, and aviation), power plants, industrial manufacturing, and agriculture.²⁻⁵ NO₂ is an
89 effective tracer for anthropogenic fuel combustion generally, and traffic specifically, especially
90 in urban areas.⁶⁻⁹ NO₂ concentration trends can be used to evaluate the efficacy of air pollution
91 regulations, as well as effects of abrupt emission changes (e.g. power plant closures, new oil and
92 gas fields, COVID-19 lockdowns).¹⁰⁻¹⁴

93 Beyond its role in PM_{2.5} and ozone formation, NO₂ itself has been associated with adverse health
94 outcomes including asthma exacerbation.^{15,16} Epidemiological studies have also found
95 associations between transportation-related air pollutants with new onset asthma in children.^{17,18}
96 While the putative agent in the traffic-related air pollution mixture remains unknown,
97 epidemiological studies are relatively consistent in their finding that NO₂ is significantly
98 associated with pediatric asthma incidence, while the evidence for other traffic-related air
99 pollutants (e.g. PM_{2.5}) is more mixed.^{17,18} Previous health impact assessments have linked NO₂
100 with ~13% of the global pediatric asthma burden, and up to ~50% in the most populated 250
101 cities worldwide.^{19,20}

102 NO_x emissions and NO₂ concentrations have changed dramatically in response to socioeconomic
103 changes and regulation, even prior to the large-scale activity changes during the COVID-19
104 pandemic.²¹⁻²⁵ In the U.S., average NO₂ concentrations dropped ~50% from the 1980s to
105 2010s,²⁶ with larger drops near major roadways²⁶ and point sources.¹⁰ In the last two decades,
106 U.S. NO_x emissions fell ~3-6% per year as vehicles got more fuel efficient and cleaner and
107 power plants shifted from coal to relatively cleaner fuels (e.g. natural gas).^{11,27,28} NO₂
108 concentrations have also decreased in Europe, though more slowly.^{29,30} In contrast, NO₂ has
109 increased in India,³¹ the Middle East,³² and Eastern Europe.²³ In China, NO_x emissions peaked
110 around 2011/2012 and subsequently declined.³³⁻³⁵

111 NO₂ pollution is a pediatric health challenge in cities, driven by higher population growth,
112 particularly in Asia and Africa where NO₂ concentrations have risen since 2000, and higher
113 asthma rates in cities compared with national averages. Previous research on NO₂ temporal

114 trends have focused on small subsets of cities and have not considered its health impacts,
115 precluding globally consistent comparisons of trends in NO₂ concentrations and associated
116 health burdens. The global coverage and long continuous record of satellite remote sensing since
117 the 1990s makes it possible to track NO₂ concentrations globally.³⁶⁻³⁹ Additionally, the high
118 spatial resolution of current satellites can capture NO₂ variation at urban and intra-urban
119 scales.^{40,41}

120 Here we investigate long-term trends of annual average NO₂ concentrations and associated
121 pediatric asthma burdens in 13,189 urban areas over the past two decades globally. We first
122 generate a new gridded global surface annual average NO₂ concentration dataset from 1990 to
123 2019 that is compatible with the spatiotemporal coverage of the Global Burden of Disease
124 (GBD) Study. We then explore trends in NO₂ concentrations and attributable pediatric asthma
125 incidence for urban areas from 2000 to 2019, for which estimated concentrations have greater
126 certainty due to available ground monitoring. Finally, we deconstruct the drivers of these trends
127 to explore the influence of NO₂ concentrations versus demographic changes.

128

129 **Methods**

130 We integrated global environmental and demographic datasets from different sources to generate
131 new estimates of surface NO₂ concentrations globally and NO₂-attributable pediatric asthma
132 incidence in cities. The analysis was done in Python (version 3.6.7).

133 *Globally gridded NO₂ concentrations*

134 We generated a new dataset of surface annual average NO₂ concentrations at 0.0083° (~1 km²)
135 resolution in five-year increments from 1990-2010 and annually from 2010-2019, consistent with
136 the GBD 2020 analysis years. We used an existing global NO₂ concentration dataset (2010-2012
137 average) at 100m resolution from a land use regression (LUR) model described by Larkin et
138 al.^{8,42} and made adjustments to correct for a high bias in rural areas and to scale concentrations to
139 additional years (Figure S1). A full description of the methods and data sources used to construct
140 the concentration dataset is in the Supplemental Material.

141 For the base year 2011, we used the Larkin et al.⁴² LUR estimates directly in all gridcells
142 categorized as “urban” according to the Global Human Settlement Model grid⁴³ or that include
143 major roadways. The LUR used annual measurements from 5,220 air monitors in 58 countries
144 (mostly in Europe, North America, and Asia) with inputs from road networks and other land use
145 variables and satellite NO₂ column observations. Globally, the model captured 54% of NO₂
146 variation, with a mean absolute error of 3.7 ppb. Model performance differed regionally: R²
147 varied from 0.42 in Africa to 0.67 in South America. In North America, Europe, and Asia, R²
148 (0.52 for each region) approximately matched the global average (0.54). For rural areas, we
149 found that the Larkin et al.⁴² dataset was biased high, and therefore adjusted concentrations using
150 surface NO₂ concentrations derived from Ozone Monitoring Instrument (OMI) satellite NO₂
151 columns (Figure S2). After adjusting the 2011 rural NO₂ concentration estimates, we scaled all
152 2011 gridcell concentrations to the GBD 2020 analysis period (1990-2019) using the MERRA-2

153 reanalysis product⁴⁴ for 1990, 1995, and 2000 and OMI NO₂ column densities for 2005-2019
154 (Figure S3).

155 As Larkin et al.⁴² demonstrated that their NO₂ concentrations agreed well with urban ground
156 observations, we added evaluations of the changes made in this work: 1) we compared our 2011
157 rural NO₂ concentration estimates to the European Monitoring and Evaluation Program (EMEP)
158 ground monitoring dataset, which has a large number of stations in rural areas, while “rural”
159 monitors in other ground monitoring networks are often located directly downwind from urban
160 areas; 2) we compared our 2019 concentrations in urban and rural areas against 4,348 monitors
161 in the U.S., Canada, and Europe.

162 While we created this spatially (all urban and rural areas globally) and temporally complete
163 (1990-2019) concentration dataset for compatibility with the GBD 2020, we focused our trend
164 analysis on urban areas over the last two decades (2000-2019), for which estimated
165 concentrations have greater certainty due to available ground monitoring.

166 NO₂-attributable pediatric asthma incidence

167 We estimated NO₂-attributable cases of pediatric asthma incidence using an epidemiologically-
168 derived concentration response function, following previous studies^{19,20} (Equation 1):

Equation 1:
$$Burden_{k,a} = \sum_{\text{Grid cells in } k} Inc_{c,a} \times Pop_{i,j,a} \times (1 - e^{-\beta X_{i,j}})$$

169

170 where *Burden* is the NO₂-attributable asthma incidence in city *k* for age group *a*, *Inc* is the
171 baseline asthma incidence rate for age group *a* and country *c*, *Pop* is the population in gridcell *i,j*
172 for age group *a*, β is the concentration response factor relating the NO₂ concentration with
173 increased risk of pediatric asthma incidence, and *X* is the annual average NO₂ concentration in
174 gridcell *i,j*. We regridged all datasets to 1km resolution and estimated NO₂-attributable asthma
175 incidence in each gridcell. We previously found that this resolution balances accuracy with
176 computational efficiency in estimating city-level NO₂-attributable disease burdens.²⁰ We sum
177 results across all gridcells within each city for a city-level total.

178 We applied a relative risk (RR) of 1.26 [95% uncertainty interval (UI): 1.1 – 1.37] per 10 ppb
179 annual average NO₂ concentration increase from a large epidemiological meta-analysis, and
180 calculated uncertainty in NO₂-attributable pediatric asthma incidence using the statistical error in
181 this RR estimate.¹⁷ As RR error is static over time it does not influence temporal trends. We used
182 a low concentration threshold of 2 ppb annual average NO₂ concentration, the 5th percentile of
183 the minimum concentrations reported by the studies in the meta-analysis. Alternative low-
184 concentration thresholds would not substantially affect estimated trends in NO₂-attributable
185 asthma incidence, since thresholds are applied uniformly across gridcells and only 3% of year-
186 specific urban concentrations were below 2 ppb.

187 We used population estimates from Worldpop⁴⁵ from 2000-2019 for ages 1-4, 5-9, 10-14, and
188 15-18 years old at ~1km resolution, and summed results across age groups for total NO₂-
189 attributable pediatric asthma incidence. National baseline annual asthma incidence rates from

190 2000-2019 were from the GBD 2019 Study. Urban area boundaries were from the GHS-SMOD
191 Urban Centre dataset for 2015 (latest year, applied here to all years).⁴³ We consider gridcells and
192 *in-situ* monitors (used to evaluate the concentration dataset) to be part of an “urban cluster” if
193 they are located in “urban” and “suburban” areas in the GHS-SMOD dataset, defined as areas
194 with >300 people per km² that are part of clusters with >5,000 people. All other gridcells and
195 monitors are considered “rural”. World regions definitions are from the GBD 2019 Study (Table
196 S2 and Figure S4).¹

197 *Drivers of change*

198 To disentangle the drivers of temporal trends in NO₂-attributable pediatric asthma incidence, we
199 isolated the contribution of exposure, population size, and baseline asthma rates using: 1) the
200 core results with annually varying data inputs, and 2) three sets of simulations in which we revert
201 one contributing parameter back to 2000 (see Supplemental Material for more details). Cohen et
202 al.⁴⁶ used a similar approach for disentangling drivers of national PM_{2.5} disease burdens. We
203 ignored interactions between the contributing factors (e.g. the influence of changing NO₂
204 concentrations on baseline asthma rates), as we considered them to be minor relative to many
205 other influences on these multi-factorial parameters (e.g. the effects of health care advances on
206 baseline asthma rates).

207 *Role of the funding source*

208 The funders of the study had no role in study design, data collection, data analysis, data
209 interpretation, or writing of the report. SA and AM had full access to all the data in the study and
210 had final responsibility for the decision to submit for publication.

211

212 **Results**

213 Our new NO₂ concentration dataset reduces the 2010-2012 Larkin et al.⁴² rural high
214 concentrations bias [mean bias (MB) reduced from 2.4 to 1.0 ppb; Table S1 and Figure S6] and
215 captures observed surface-level concentrations in both urban and rural areas in 2019 (MB = 3.3,
216 1.7, and 2.3 in Canada, U.S., and Europe, respectively; Figure S7). See the Supplemental
217 Material for further evaluation description and results. Estimated NO₂ concentrations are highest
218 in the most populated regions of the world, including North America, Europe, and South and
219 East Asia throughout the time period (Figure 1). Cities with the 10 highest NO₂ concentrations in
220 2019 were located in the Middle East (Lebanon, Iraq, Iran), China, and Russia (Figure S8).

221 We estimated that the global population-weighted average annual mean NO₂ concentration was
222 6.6 ppb in 2019, leading to 1.85 million (95% UI: 0.93 – 2.8 million) new asthma cases among
223 children worldwide that year, or 8.5% (95% UI: 4.3% – 12.8%) of all pediatric asthma incidence
224 (Figure 2). Approximately two-thirds of NO₂-attributable pediatric asthma incidence occurred in
225 the 13,189 urban areas (1.22 million cases; 95% UI: 0.60 – 1.8 million). Compared with rural
226 areas, urban areas had 2-4 times higher population-weighted NO₂ concentrations (10.6 ppb in
227 urban areas versus 4.2 ppb in rural areas), NO₂-attributable asthma cases (1.22 million versus

228 0.63 million), NO₂-attributable asthma cases per 100,000 (156 versus 40), and attributable
229 fractions (16.4% versus 4.5%) in 2019.

230 Focusing on urban areas in the last two decades, we found that annual average NO₂
231 concentrations decreased by 13%, from 12.2 ppb in 2000 to 10.6 ppb in 2019, with a steady
232 decline from 2011 to 2019 after rising from 2000 to 2011 (Figure 2). NO₂ concentrations in
233 High-income cities exceeded the global average throughout the time period, despite declining
234 38% from 17.6 ppb in 2000 to 11.0 ppb in 2019 (Figure 3). Contrastingly, concentrations in
235 South Asia and Sub-Saharan Africa rose by 18% (8.6 to 10.1 ppb) and 11% (6.4 to 7.1 ppb),
236 respectively, but remained lower than the global urban average throughout the time period.
237 These large regional groupings of cities obscure contrasting trends between sub-regions in some
238 cases (Figure S9).

239 We estimated that ~1.2 million pediatric asthma cases in urban areas globally were attributable to
240 NO₂ pollution in both 2000 and 2019, though the rate per 100,000 children declined 14% from
241 176 to 156 per 100,000 children as the urban pediatric population grew by 12% (Figure 2). High-
242 income cities had the most NO₂-attributable asthma incidence in 2019, with 341,000 cases or
243 28% of the global urban total, despite having only 14% of the global urban pediatric population
244 (Figure 4 and Table S4). While total NO₂-attributable pediatric asthma cases were in the most
245 populated cities of the world (Figure S10), all 10 highest attributable rates were in the U.S.
246 (Figure S11). Contrastingly, cities in South Asia, with approximately a quarter of the global
247 pediatric population, only accounted for 7% of global urban NO₂-attributable pediatric asthma
248 incidence. NO₂-attributable pediatric asthma incidence rates were also highest in the High-
249 income region (311 attributable cases per 100,000 children) and were an order of magnitude
250 lower in South Asia (50).

251 The fraction of pediatric asthma incidence that was estimated to be attributable to NO₂ across all
252 13,189 urban areas globally dropped from 19.7% in 2000 to 16.4% in 2019 (Figure 2). Urban
253 attributable fractions dropped between 2000 and 2019 in High-income (-41%), Latin America
254 and Caribbean (-16%), Central Europe, Eastern Europe, and Central Asia (-13%), and Southeast
255 Asia, East Asia, and Oceania (-6%) regions, and rose in South Asia (+23%), Sub-Saharan Africa
256 (+11%), and North Africa and Middle East (+5%) regions. The large decrease in High-income
257 cities is partly driven by even larger drops in North America (-52%; Figure S8). The 35%
258 increase in Central Europe, Eastern Europe, and Central Asia was driven by >50% increases in
259 Central Asia and Eastern Europe, balanced by a 14% decrease in Central Europe. In 2019,
260 regional urban average attributable fractions ranged from 10% in Sub-Saharan Africa to 20% in
261 Central Europe, Eastern Europe, and Central Asia and North Africa and Middle East. As for
262 concentrations, the 10 highest attributable fractions were located in Lebanon, Iraq, Iran, China,
263 and Russia (Figure S11).

264 Estimated temporal trends in urban NO₂-attributable pediatric asthma incidence are driven by
265 simultaneous and often competing changes in NO₂ concentrations, pediatric population, and
266 asthma incidence rates (Figure 5). Australasia and High-income Asia Pacific are the only regions
267 where declining concentrations, pediatric population size, and asthma rates all contribute to
268 overall drops in NO₂-attributable pediatric asthma incidence. The opposite occurred in Central,

269 South, and Southeast Asia, and in North Africa and the Middle East, where concentrations,
270 pediatric population, and asthma rates all rose. In High-income North America, Western Europe,
271 and several other regions, declining NO₂ concentrations were offset by increases in asthma
272 incidence rates and/or pediatric population size. These competing influences changed over time,
273 with declining concentrations becoming more influential over time in North America and
274 Southern Latin America, and population growth becoming more influential in North Africa and
275 Middle East and Southern Sub-Saharan Africa (Figure S12).

276

277 **Discussion**

278 We estimated that 1.84 million (95% UI: 0.93 – 2.8 million) pediatric asthma cases globally
279 could be attributable to NO₂ pollution in 2019. Despite having only one-third of the global
280 pediatric population, urban areas had two-thirds of NO₂-attributable pediatric asthma incidence.
281 The NO₂-attributable fraction of pediatric asthma incidence in urban areas globally declined
282 from 20% in 2000 to 16% in 2019. Regional trends were inconsistent: urban average attributable
283 fractions dropped in High-income cities; Latin America and Caribbean; Central Europe, Eastern
284 Europe, and Central Asia; and Southeast Asia, East Asia, and Oceania, and rose in South Asia;
285 Sub-Saharan Africa; and North Africa and Middle East. The drivers of temporal trends in NO₂
286 concentrations and pediatric asthma burdens were also inconsistent regionally, with declining
287 NO₂ concentrations in some regions counteracted by increases in pediatric population size and
288 asthma incidence rates.

289 Our study is consistent with the broader literature demonstrating that NO₂ is largely an urban
290 pollutant.^{7,47–49} Estimated NO₂ concentration trends are consistent with recent studies using
291 satellite data to investigate NO₂ concentration trends during 2004-2018 for the U.S., Europe,
292 China, India, and Japan.^{23,31,50} For example, Qu et al.⁵¹ also showed a similar decrease in U.S.
293 NO₂ concentrations based on ground observations, satellite data, and modeling outputs from
294 2006-2016, and Henneman et al.²⁶ showed a similar decrease using ground observations from
295 1980-2020. A recent study focused on biomass burning in the equatorial Africa region found
296 declining concentrations from 2005 to 2017⁵², while we found an increase in Sub-Saharan Africa
297 from 2000-2019. A biomass burning decline in the region may be smaller and offset by
298 anthropogenic emission changes in populated urban areas.

299 While our new NO₂ dataset leverages advantages of different data sources, concentrations
300 remain uncertain. Many cities, particularly in low- and middle-income countries (LMICs), still
301 lack ground NO₂ monitors, challenging calibration and evaluation of LUR models.⁴² Urban NO₂
302 concentrations are therefore more certain in North America, Europe, and Asia, compared with
303 Africa and South America. Rural concentrations are uncertain globally with limited ground
304 monitoring outside of urban areas. Scaling the 2010-2012 LUR NO₂ concentrations to other
305 years assumes that the land use predictors are static over time. This assumption is likely
306 supported by slow changes in road density and volume and urban form, but over the two decades
307 explored here, some land use evolution is likely⁵³, particularly in rapidly developing LMICs. The
308 directional impact of these uncertainties on results is unknown.

309 Our estimate of the global burden of NO₂ on pediatric asthma incidence in 2019 is less than half
310 of the 4.2 million found by Achakulwisut et al.¹⁹ for 2015. Our results for India are also lower
311 than previous estimates while our U.S. results are higher.^{17,20} Several factors explain this
312 discrepancy. First, our new NO₂ concentrations correct for a high rural NO₂ bias, leading to
313 lower NO₂-attributable asthma incidence estimates, especially in countries with larger rural
314 populations (e.g. India). Second, GBD 2019 baseline asthma rates are much lower than in
315 previous versions, except in high income areas (e.g. U.S.), due to a change in the case definition
316 used which lowered estimated rates in most places and raised them for the U.S.⁵⁴ For example,
317 baseline pediatric asthma incidence rates in 2015 (the year analyzed by Mohegh et al.²⁰) in the
318 GBD 2019 were 81% of GBD 2017 values. Contrastingly, U.S. pediatric asthma incidence rates
319 were a factor of 2.2 higher in the GBD 2019 versus GBD 2017. Changes in baseline asthma rates
320 approximately proportionally affect estimated NO₂-attributable pediatric asthma incidence. Our
321 NO₂ attributable fraction result in High-Income North America in 2019 (17.3%) was similar to a
322 previous estimate for the U.S. in 2000 (17.9%), though our NO₂ concentrations were lower (10.9
323 ppb in urban areas vs. 13.2 ppb overall).⁴⁷ The different analysis years are important since, as we
324 have shown, NO₂ concentrations trends are changing rapidly.

325 The health impact assessment method also introduces uncertainties. While we used national
326 pediatric asthma rates, asthma prevalence varies within countries.⁴⁷ Living in urban areas has
327 been associated with increased risk of asthma prevalence in LMICs⁵⁵ and asthma-related
328 emergency department visits and hospitalizations in the U.S.⁵⁶ Similarly, temporal trends in
329 baseline asthma incidence may differ in urban areas compared with national averages, especially
330 in rapidly urbanizing LMICs. If asthma prevalence is higher in urban areas compared with
331 national averages, NO₂-attributable asthma incidence may be underestimated. In addition, it is
332 currently unknown whether pediatric asthma incidence is associated with NO₂, the traffic-related
333 air pollution mixture, or the broader combustion-related air pollution mixture. Finally, the 1km
334 resolution of our NO₂ concentration estimates may not capture areas with co-located steep spatial
335 gradients in concentrations and population, potentially leading NO₂-attributable asthma
336 incidence to be underestimated.

337 Despite these uncertainties and limitations, our results demonstrate the important influence of
338 combustion-related air pollution on children's health in cities globally. In places that have
339 effective air quality management programs (e.g. U.S., Europe), NO₂ concentrations have been
340 trending downward for decades, with benefits for children's respiratory health. Even with these
341 improvements, current NO₂ levels contribute substantially to pediatric asthma incidence,
342 highlighting that mitigating air pollution should be a critical element of children's public health
343 strategies. For cities that have not benefited from strong local or national-scale air quality
344 management programs, the experience of cities that have such programs demonstrates that
345 addressing combustion-related air pollution can lead to major air quality and public health
346 improvements over relatively short time frames (years). These air quality improvements can be
347 achieved through either end-of-pipe emission control technologies such as catalytic converters or
348 avoiding the combustion in the first place, which would have additional benefits from reduced
349 greenhouse gas emissions.

350 Our study demonstrates the value of satellite remote sensing and statistical models for tracking
351 NO₂ pollution and for environmental health surveillance at local, national, and global scales. The
352 combination of methods offers strengths beyond the capabilities of each technique alone: a long
353 and consistent observational record of NO₂ column densities from satellites with the high spatial
354 resolution of surface concentration predictions from LUR models. Future studies may leverage
355 these data sources and others, including new satellite sensors that have higher temporal and
356 spatial resolutions, mobile monitoring, distributed ground sensor networks, and chemical
357 transport models, to further improve the accuracy and spatiotemporal resolution of NO₂
358 concentration estimates. Further, our study shows the importance of considering demographic
359 changes over time for understanding air pollution health risks. Improved and more widely
360 accessible information about disease rates, and capturing population distribution and movement,
361 will enable more accurate and highly resolved air pollution health impact assessments.

362

363

364 **References**

- 365 (1) GBD 2019 Risk Factor Collaborators. Global Burden of 87 Risk Factors in 204 Countries
 366 and Territories, 1990–2019: A Systematic Analysis for the Global Burden of Disease Study
 367 2019. *The Lancet* **2020**, *396* (10258), 1223–1249. [https://doi.org/10.1016/S0140-](https://doi.org/10.1016/S0140-6736(20)30752-2)
 368 [6736\(20\)30752-2](https://doi.org/10.1016/S0140-6736(20)30752-2).
- 369 (2) McDuffie, E. E.; Smith, S. J.; O’Rourke, P.; Tibrewal, K.; Venkataraman, C.; Marais, E.
 370 A.; Zheng, B.; Crippa, M.; Brauer, M.; Martin, R. V. A Global Anthropogenic Emission
 371 Inventory of Atmospheric Pollutants from Sector- and Fuel-Specific Sources (1970–2017):
 372 An Application of the Community Emissions Data System (CEDS). *Earth Syst. Sci. Data*
 373 **2020**, *12* (4), 3413–3442. <https://doi.org/10.5194/essd-12-3413-2020>.
- 374 (3) Anenberg, S.; Miller, J.; Minjares, R.; Du, L.; Henze, D. K.; Lacey, F.; Malley, C. S.;
 375 Emberson, L.; Franco, V.; Klimont, Z.; Heyes, C. Impacts and Mitigation of Excess Diesel-
 376 Related NOx Emissions in 11 Major Vehicle Markets. *Nature* **2017**, *545*, 467–471.
 377 <https://doi.org/10.1038/nature22086>.
- 378 (4) Stohl, A.; Aamaas, B.; Amann, M.; Baker, L. H.; Bellouin, N.; Berntsen, T. K.; Boucher,
 379 O.; Cherian, R.; Collins, W.; Daskalakis, N.; Dusinska, M.; Eckhardt, S.; Fuglestvedt, J. S.;
 380 Harju, M.; Heyes, C.; Hodnebrog, ø.; Hao, J.; Im, U.; Kanakidou, M.; Klimont, Z.;
 381 Kupiainen, K.; Law, K. S.; Lund, M. T.; Maas, R.; MacIntosh, C. R.; Myhre, G.;
 382 Myriokefalitakis, S.; Olivie, D.; Quaas, J.; Quennehen, B.; Raut, J.-C.; Rumbold, S. T.;
 383 Samset, B. H.; Schulz, M.; Seland, ø.; Shine, K. P.; Skeie, R. B.; Wang, S.; Yttri, K. E.;
 384 Zhu, T. Evaluating the Climate and Air Quality Impacts of Short-Lived Pollutants.
 385 *Atmospheric Chem. Phys.* **2015**, *15* (18), 10529–10566. [https://doi.org/10.5194/acp-15-](https://doi.org/10.5194/acp-15-10529-2015)
 386 [10529-2015](https://doi.org/10.5194/acp-15-10529-2015).
- 387 (5) Crippa, M.; Guizzardi, D.; Muntean, M.; Schaaf, E.; Dentener, F.; van Aardenne, J. A.;
 388 Monni, S.; Doering, U.; Olivier, J. G. J.; Pagliari, V.; Janssens-Maenhout, G. Gridded
 389 Emissions of Air Pollutants for the Period 1970–2012 within EDGAR v4.3.2. *Earth Syst.*
 390 *Sci. Data* **2018**, *10* (4), 1987–2013. <https://doi.org/10.5194/essd-10-1987-2018>.
- 391 (6) Stavrou, T.; Müller, J.-F.; Boersma, K. F.; De Smedt, I.; van der A, R. J. Assessing the
 392 Distribution and Growth Rates of NOx Emission Sources by Inverting a 10-Year Record of
 393 NOx Satellite Columns. *Geophys. Res. Lett.* **2008**, *35* (10).
 394 <https://doi.org/10.1029/2008GL033521>.
- 395 (7) Bechle, M. J.; Millet, D. B.; Marshall, J. D. Effects of Income and Urban Form on Urban
 396 NO2: Global Evidence from Satellites. *Environ. Sci. Technol.* **2011**, *45* (11), 4914–4919.
 397 <https://doi.org/10.1021/es103866b>.
- 398 (8) Geddes, J. A.; Martin, R. V.; Boys, B. L.; van Donkelaar, A. Long-Term Trends Worldwide
 399 in Ambient NO2 Concentrations Inferred from Satellite Observations. *Environ. Health*
 400 *Perspect.* **2016**, *124* (3), 281–289. <https://doi.org/10.1289/ehp.1409567>.
- 401 (9) Bechle, M. J.; Millet, D. B.; Marshall, J. D. Does Urban Form Affect Urban NO2? Satellite-
 402 Based Evidence for More than 1200 Cities. *Environ. Sci. Technol.* **2017**, *51* (21), 12707–
 403 12716. <https://doi.org/10.1021/acs.est.7b01194>.
- 404 (10) Duncan, B. N.; Yoshida, Y.; de Foy, B.; Lamsal, L. N.; Streets, D. G.; Lu, Z.; Pickering, K.
 405 E.; Krotkov, N. A. The Observed Response of Ozone Monitoring Instrument (OMI) NO2
 406 Columns to NOx Emission Controls on Power Plants in the United States: 2005–2011.
 407 *Atmos. Environ.* **2013**, *81*, 102–111. <https://doi.org/10.1016/j.atmosenv.2013.08.068>.
- 408 (11) Silvern, R. F.; Jacob, D. J.; Mickley, L. J.; Sulprizio, M. P.; Travis, K. R.; Marais, E. A.;
 409 Cohen, R. C.; Laughner, J. L.; Choi, S.; Joiner, J.; Lamsal, L. N. Using Satellite

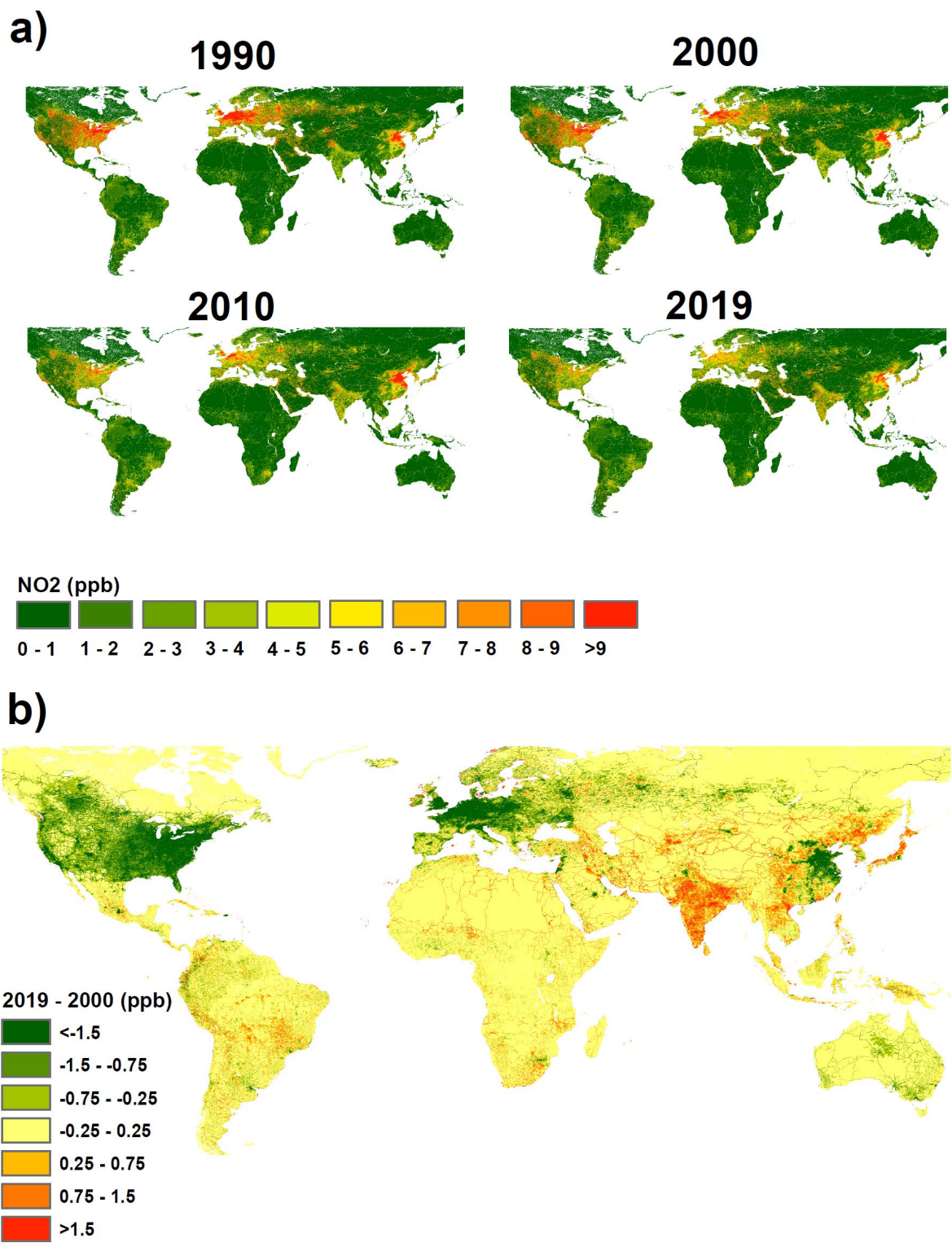
- 410 Observations of Tropospheric NO₂ Columns to Infer Long-Term Trends in US NO_x
411 Emissions: The Importance of Accounting for the Free Tropospheric NO₂ Background.
412 *Atmospheric Chem. Phys.* **2019**, *19* (13), 8863–8878. [https://doi.org/10.5194/acp-19-8863-](https://doi.org/10.5194/acp-19-8863-2019)
413 2019.
- 414 (12) Dix, B.; Bruin, J.; Roosenbrand, E.; Vlemmix, T.; Francoeur, C.; Gorchov-Negron, A.;
415 McDonald, B.; Zhizhin, M.; Elvidge, C.; Veefkind, P.; Levelt, P.; Gouw, J. Nitrogen Oxide
416 Emissions from U.S. Oil and Gas Production: Recent Trends and Source Attribution.
417 *Geophys. Res. Lett.* **2020**, *47* (1). <https://doi.org/10.1029/2019GL085866>.
- 418 (13) Goldberg, D. L.; Anenberg, S. C.; Griffin, D.; McLinden, C. A.; Lu, Z.; Streets, D. G.
419 Disentangling the Impact of the COVID-19 Lockdowns on Urban NO₂ From Natural
420 Variability. *Geophys. Res. Lett.* **2020**, *47* (17). <https://doi.org/10.1029/2020GL089269>.
- 421 (14) Kerr, G. H.; Goldberg, D. L.; Anenberg, S. C. COVID-19 Pandemic Reveals Persistent
422 Disparities in Nitrogen Dioxide Pollution. *Proc. Natl. Acad. Sci.* **2021**, *In press*.
- 423 (15) Perez, L.; Lurmann, F.; Wilson, J.; Pastor, M.; Brandt, S. J.; Künzli, N.; McConnell, R.
424 Near-Roadway Pollution and Childhood Asthma: Implications for Developing “Win–Win”
425 Compact Urban Development and Clean Vehicle Strategies. *Environ. Health Perspect.*
426 **2012**, *120* (11), 1619–1626. <https://doi.org/10.1289/ehp.1104785>.
- 427 (16) Gauderman, W. J.; Avol, E.; Lurmann, F.; Kuenzli, N.; Gilliland, F.; Peters, J.; McConnell,
428 R. Childhood Asthma and Exposure to Traffic and Nitrogen Dioxide: *Epidemiology* **2005**,
429 *16* (6), 737–743. <https://doi.org/10.1097/01.ede.0000181308.51440.75>.
- 430 (17) Khreis, H.; Kelly, C.; Tate, J.; Parslow, R.; Lucas, K.; Nieuwenhuijsen, M. Exposure to
431 Traffic-Related Air Pollution and Risk of Development of Childhood Asthma: A
432 Systematic Review and Meta-Analysis. *Environ. Int.* **2017**, *100*, 1–31.
433 <https://doi.org/10.1016/j.envint.2016.11.012>.
- 434 (18) Anenberg, S. C.; Henze, D. K.; Tinney, V.; Kinney, P. L.; Raich, W.; Fann, N.; Malley, C.
435 S.; Roman, H.; Lamsal, L.; Duncan, B.; Martin, R. V.; van Donkelaar, A.; Brauer, M.;
436 Doherty, R.; Jonson, J. E.; Davila, Y.; Sudo, K.; Kuylensstierna, J. C. I. Estimates of the
437 Global Burden of Ambient PM_{2.5}, Ozone, and NO₂ on Asthma Incidence and Emergency
438 Room Visits. *Environ. Health Perspect.* **2018**, *126* (10), 107004.
439 <https://doi.org/10.1289/EHP3766>.
- 440 (19) Achakulwisut, P.; Brauer, M.; Hystad, P.; Anenberg, S. C. Global, National, and Urban
441 Burdens of Paediatric Asthma Incidence Attributable to Ambient NO₂ Pollution: Estimates
442 from Global Datasets. *Lancet Planet. Health* **2019**, *3* (4), e166–e178.
443 [https://doi.org/10.1016/S2542-5196\(19\)30046-4](https://doi.org/10.1016/S2542-5196(19)30046-4).
- 444 (20) Mohegh, A.; Goldberg, D.; Achakulwisut, P.; Anenberg, S. C. Sensitivity of Estimated
445 NO₂-Attributable Pediatric Asthma Incidence to Grid Resolution and Urbanicity. *Environ.*
446 *Res. Lett.* **2020**, *16* (1), 014019. <https://doi.org/10.1088/1748-9326/abce25>.
- 447 (21) Lamsal, L. N.; Duncan, B. N.; Yoshida, Y.; Krotkov, N. A.; Pickering, K. E.; Streets, D. G.;
448 Lu, Z. U.S. NO₂ Trends (2005–2013): EPA Air Quality System (AQS) Data versus
449 Improved Observations from the Ozone Monitoring Instrument (OMI). *Atmos. Environ.*
450 **2015**, *110*, 130–143. <https://doi.org/10.1016/j.atmosenv.2015.03.055>.
- 451 (22) Miyazaki, K.; Eskes, H.; Sudo, K.; Boersma, K. F.; Bowman, K.; Kanaya, Y. Decadal
452 Changes in Global Surface NO_x Emissions from Multi-Constituent Satellite Data
453 Assimilation. *Atmospheric Chem. Phys.* **2017**, *17* (2), 807–837. [https://doi.org/10.5194/acp-](https://doi.org/10.5194/acp-17-807-2017)
454 17-807-2017.

- 455 (23) Georgoulias, A. K.; van der A, R. J.; Stammes, P.; Boersma, K. F.; Eskes, H. J. Trends and
456 Trend Reversal Detection in 2 Decades of Tropospheric NO₂ Satellite Observations.
457 *Atmospheric Chem. Phys.* **2019**, *19* (9), 6269–6294. [https://doi.org/10.5194/acp-19-6269-](https://doi.org/10.5194/acp-19-6269-2019)
458 2019.
- 459 (24) Tong, D. Q.; Lamsal, L.; Pan, L.; Ding, C.; Kim, H.; Lee, P.; Chai, T.; Pickering, K. E.;
460 Stajner, I. Long-Term NO_x Trends over Large Cities in the United States during the Great
461 Recession: Comparison of Satellite Retrievals, Ground Observations, and Emission
462 Inventories. *Atmos. Environ.* **2015**, *107*, 70–84.
463 <https://doi.org/10.1016/j.atmosenv.2015.01.035>.
- 464 (25) Kharol, S. K.; Martin, R. V.; Philip, S.; Boys, B.; Lamsal, L. N.; Jerrett, M.; Brauer, M.;
465 Crouse, D. L.; McLinden, C.; Burnett, R. T. Assessment of the Magnitude and Recent
466 Trends in Satellite-Derived Ground-Level Nitrogen Dioxide over North America. *Atmos.*
467 *Environ.* **2015**, *118*, 236–245. <https://doi.org/10.1016/j.atmosenv.2015.08.011>.
- 468 (26) Henneman, L. R. F.; Shen, H.; Hogrefe, C.; Russell, A. G.; Zigler, C. M. Four Decades of
469 United States Mobile Source Pollutants: Spatial–Temporal Trends Assessed by Ground-
470 Based Monitors, Air Quality Models, and Satellites. *Environ. Sci. Technol.* **2021**, *55* (2),
471 882–892. <https://doi.org/10.1021/acs.est.0c07128>.
- 472 (27) Goldberg, D. L.; Lu, Z.; Oda, T.; Lamsal, L. N.; Liu, F.; Griffin, D.; McLinden, C. A.;
473 Krotkov, N. A.; Duncan, B. N.; Streets, D. G. Exploiting OMI NO₂ Satellite Observations
474 to Infer Fossil-Fuel CO₂ Emissions from U.S. Megacities. *Sci. Total Environ.* **2019**, *695*,
475 133805. <https://doi.org/10.1016/j.scitotenv.2019.133805>.
- 476 (28) Zhang, R.; Wang, Y.; Smeltzer, C.; Qu, H.; Koshak, W.; Boersma, K. F. Comparing OMI-
477 Based and EPA AQS in Situ NO₂ Trends: Towards Understanding Surface NO_x Emission
478 Changes. *Atmospheric Meas. Tech.* **2018**, *11* (7), 3955–3967. [https://doi.org/10.5194/amt-](https://doi.org/10.5194/amt-11-3955-2018)
479 11-3955-2018.
- 480 (29) Curier, R. L.; Kranenburg, R.; Segers, A. J. S.; Timmermans, R. M. A.; Schaap, M.
481 Synergistic Use of OMI NO₂ Tropospheric Columns and LOTOS–EUROS to Evaluate the
482 NO_x Emission Trends across Europe. *Remote Sens. Environ.* **2014**, *149*, 58–69.
483 <https://doi.org/10.1016/j.rse.2014.03.032>.
- 484 (30) Zara, M.; Boersma, K. F.; Eskes, H.; Denier van der Gon, H.; Vilà-Guerau de Arellano, J.;
485 Krol, M.; van der Swaluw, E.; Schuch, W.; Velders, G. J. M. Reductions in Nitrogen
486 Oxides over the Netherlands between 2005 and 2018 Observed from Space and on the
487 Ground: Decreasing Emissions and Increasing O₃ Indicate Changing NO_x Chemistry.
488 *Atmospheric Environ. X* **2021**, *9*, 100104. <https://doi.org/10.1016/j.aeaoa.2021.100104>.
- 489 (31) Itahashi, S.; Yumimoto, K.; Kurokawa, J.; Morino, Y.; Nagashima, T.; Miyazaki, K.; Maki,
490 T.; Ohara, T. Inverse Estimation of NO_x Emissions over China and India 2005–2016:
491 Contrasting Recent Trends and Future Perspectives. *Environ. Res. Lett.* **2019**, *14* (12),
492 124020. <https://doi.org/10.1088/1748-9326/ab4d7f>.
- 493 (32) Barkley, M. P.; González Abad, G.; Kurosu, T. P.; Spurr, R.; Torbatian, S.; Lerot, C. OMI
494 Air-Quality Monitoring over the Middle East. *Atmospheric Chem. Phys.* **2017**, *17* (7),
495 4687–4709. <https://doi.org/10.5194/acp-17-4687-2017>.
- 496 (33) de Foy, B.; Lu, Z.; Streets, D. G. Satellite NO₂ Retrievals Suggest China Has Exceeded Its
497 NO_x Reduction Goals from the Twelfth Five-Year Plan. *Sci. Rep.* **2016**, *6* (1), 35912.
498 <https://doi.org/10.1038/srep35912>.
- 499 (34) Liu, F.; Beirle, S.; Zhang, Q.; van der A, R. J.; Zheng, B.; Tong, D.; He, K. NO_x Emission
500 Trends over Chinese Cities Estimated from OMI Observations during 2005 to 2015.

- 501 *Atmospheric Chem. Phys.* **2017**, *17* (15), 9261–9275. [https://doi.org/10.5194/acp-17-9261-](https://doi.org/10.5194/acp-17-9261-2017)
502 2017.
- 503 (35) Zheng, B.; Tong, D.; Li, M.; Liu, F.; Hong, C.; Geng, G.; Li, H.; Li, X.; Peng, L.; Qi, J.;
504 Yan, L.; Zhang, Y.; Zhao, H.; Zheng, Y.; He, K.; Zhang, Q. Trends in China's
505 Anthropogenic Emissions since 2010 as the Consequence of Clean Air Actions.
506 *Atmospheric Chem. Phys.* **2018**, *18* (19), 14095–14111. [https://doi.org/10.5194/acp-18-](https://doi.org/10.5194/acp-18-14095-2018)
507 14095-2018.
- 508 (36) Leue, C.; Wenig, M.; Wagner, T.; Klimm, O.; Platt, U.; Jähne, B. Quantitative Analysis of
509 NO_x Emissions from Global Ozone Monitoring Experiment Satellite Image Sequences. *J.*
510 *Geophys. Res. Atmospheres* **2001**, *106* (D6), 5493–5505.
511 <https://doi.org/10.1029/2000JD900572>.
- 512 (37) van der A, R. J.; Eskes, H. J.; Boersma, K. F.; van Noije, T. P. C.; Van Roozendaal, M.; De
513 Smedt, I.; Peters, D. H. M. U.; Meijer, E. W. Trends, Seasonal Variability and Dominant
514 NO_x Source Derived from a Ten Year Record of NO₂ Measured from Space. *J. Geophys.*
515 *Res.* **2008**, *113* (D4), D04302. <https://doi.org/10.1029/2007JD009021>.
- 516 (38) Duncan, B. N.; Lamsal, L. N.; Thompson, A. M.; Yoshida, Y.; Lu, Z.; Streets, D. G.;
517 Hurwitz, M. M.; Pickering, K. E. A Space-Based, High-Resolution View of Notable
518 Changes in Urban NO_x Pollution around the World (2005-2014). *J. Geophys. Res.*
519 *Atmospheres* **2016**, *121* (2), 976–996. <https://doi.org/10.1002/2015JD024121>.
- 520 (39) Anenberg, S. C.; Bindl, M.; Brauer, M.; Castillo, J. J.; Cavalieri, S.; Duncan, B. N.; Fiore,
521 A. M.; Fuller, R.; Goldberg, D. L.; Henze, D. K.; Hess, J.; Holloway, T.; James, P.; Jin, X.;
522 Kheirbek, I.; Kinney, P. L.; Liu, Y.; Mohegh, A.; Patz, J.; Jimenez, M. P.; Roy, A.; Tong,
523 D.; Walker, K.; Watts, N.; West, J. J. Using Satellites to Track Indicators of Global Air
524 Pollution and Climate Change Impacts: Lessons Learned from a NASA-supported Science-
525 stakeholder Collaborative. *GeoHealth* **2020**. <https://doi.org/10.1029/2020GH000270>.
- 526 (40) Griffin, D.; Zhao, X.; McLinden, C. A.; Boersma, F.; Bourassa, A.; Dammers, E.;
527 Degenstein, D.; Eskes, H.; Fehr, L.; Fioletov, V.; Hayden, K.; Kharol, S. K.; Li, S.; Makar,
528 P.; Martin, R. V.; Mihele, C.; Mittermeier, R. L.; Krotkov, N.; Sneep, M.; Lamsal, L. N.;
529 Linden, M. ter; Geffen, J. van; Veefkind, P.; Wolde, M. High-Resolution Mapping of
530 Nitrogen Dioxide With TROPOMI: First Results and Validation Over the Canadian Oil
531 Sands. *Geophys. Res. Lett.* **2019**, *46* (2), 1049–1060.
532 <https://doi.org/10.1029/2018GL081095>.
- 533 (41) Goldberg, D. L.; Anenberg, S. C.; Kerr, G. H.; Mohegh, A.; Lu, Z.; Streets, D. G.
534 TROPOMI NO₂ in the United States: A Detailed Look at the Annual Averages, Weekly
535 Cycles, Effects of Temperature, and Correlation With Surface NO₂ Concentrations. *Earths*
536 *Future* **2021**, *9* (4). <https://doi.org/10.1029/2020EF001665>.
- 537 (42) Larkin, A.; Geddes, J. A.; Martin, R. V.; Xiao, Q.; Liu, Y.; Marshall, J. D.; Brauer, M.;
538 Hystad, P. Global Land Use Regression Model for Nitrogen Dioxide Air Pollution.
539 *Environ. Sci. Technol.* **2017**, *51* (12), 6957–6964. <https://doi.org/10.1021/acs.est.7b01148>.
- 540 (43) Pesaresi, M.; Florczyk, A.; Schiavina, M.; Melchiorri, M.; Maffeni, L. GHS Settlement
541 Grid, Updated and Refined REGIO Model 2014 in Application to GHS-BUILT R2018A
542 and GHS-POP R2019A, Multitemporal (1975-1990-2000-2015), R2019A, 2019.
543 <https://doi.org/10.2905/42E8BE89-54FF-464E-BE7B-BF9E64DA5218>.
- 544 (44) Gelaro, R.; McCarty, W.; Suárez, M. J.; Todling, R.; Molod, A.; Takacs, L.; Randles, C. A.;
545 Darmenov, A.; Bosilovich, M. G.; Reichle, R.; Wargan, K.; Coy, L.; Cullather, R.; Draper,
546 C.; Akella, S.; Buchard, V.; Conaty, A.; da Silva, A. M.; Gu, W.; Kim, G.-K.; Koster, R.;

- 547 Lucchesi, R.; Merkova, D.; Nielsen, J. E.; Partyka, G.; Pawson, S.; Putman, W.; Rienecker,
548 M.; Schubert, S. D.; Sienkiewicz, M.; Zhao, B. The Modern-Era Retrospective Analysis for
549 Research and Applications, Version 2 (MERRA-2). *J. Clim.* **2017**, *30* (14), 5419–5454.
550 <https://doi.org/10.1175/JCLI-D-16-0758.1>.
- 551 (45) Tatem, A. J. WorldPop, Open Data for Spatial Demography. *Sci. Data* **2017**, *4* (1), 170004.
552 <https://doi.org/10.1038/sdata.2017.4>.
- 553 (46) Cohen, A. J.; Brauer, M.; Burnett, R.; Anderson, H. R.; Frostad, J.; Estep, K.; Balakrishnan,
554 K.; Brunekreef, B.; Dandona, L.; Dandona, R.; Feigin, V.; Freedman, G.; Hubbell, B.;
555 Jobling, A.; Kan, H.; Knibbs, L.; Liu, Y.; Martin, R.; Morawska, L.; Pope, C. A.; Shin, H.;
556 Straif, K.; Shaddick, G.; Thomas, M.; van Dingenen, R.; van Donkelaar, A.; Vos, T.;
557 Murray, C. J. L.; Forouzanfar, M. H. Estimates and 25-Year Trends of the Global Burden of
558 Disease Attributable to Ambient Air Pollution: An Analysis of Data from the Global
559 Burden of Diseases Study 2015. *The Lancet* **2017**. [https://doi.org/10.1016/S0140-](https://doi.org/10.1016/S0140-6736(17)30505-6)
560 [6736\(17\)30505-6](https://doi.org/10.1016/S0140-6736(17)30505-6).
- 561 (47) Khreis, H.; Alotaibi, R.; Horney, J.; McConnell, R. The Impact of Baseline Incidence Rates
562 on Burden of Disease Assessment of Air Pollution and Onset Childhood Asthma: Analysis
563 of Data from the Contiguous United States. *Ann. Epidemiol.* **2021**, *53*, 76-88.e10.
564 <https://doi.org/10.1016/j.annepidem.2020.08.063>.
- 565 (48) Bechle, M. J.; Millet, D. B.; Marshall, J. D. National Spatiotemporal Exposure Surface for
566 NO₂: Monthly Scaling of a Satellite-Derived Land-Use Regression, 2000–2010. *Environ.*
567 *Sci. Technol.* **2015**, *49* (20), 12297–12305. <https://doi.org/10.1021/acs.est.5b02882>.
- 568 (49) Lee, H. J.; Koutrakis, P. Daily Ambient NO₂ Concentration Predictions Using Satellite
569 Ozone Monitoring Instrument NO₂ Data and Land Use Regression. *Environ. Sci. Technol.*
570 **2014**, 140204134232009. <https://doi.org/10.1021/es404845f>.
- 571 (50) Jamali, S.; Klingmyr, D.; Tagesson, T. Global-Scale Patterns and Trends in Tropospheric
572 NO₂ Concentrations, 2005–2018. *Remote Sens.* **2020**, *12* (21), 3526.
573 <https://doi.org/10.3390/rs12213526>.
- 574 (51) Qu, Z.; Henze, D. K.; Cooper, O. R.; Neu, J. L. *Improving NO₂ and Ozone Simulations*
575 *through Global NO_x Emission Inversions*; preprint; Gases/Atmospheric
576 Modelling/Troposphere/Chemistry (chemical composition and reactions), 2020.
577 <https://doi.org/10.5194/acp-2020-307>.
- 578 (52) Hickman, J. E.; Andela, N.; Tsigaridis, K.; Galy-Lacaux, C.; Ossouhou, M.; Bauer, S. E.
579 Reductions in NO₂ Burden over North Equatorial Africa from Decline in Biomass Burning
580 in Spite of Growing Fossil Fuel Use, 2005 to 2017. *Proc. Natl. Acad. Sci.* **2021**, *118* (7),
581 e2002579118. <https://doi.org/10.1073/pnas.2002579118>.
- 582 (53) Barrington-Leigh, C.; Millard-Ball, A. Global Trends toward Urban Street-Network
583 Sprawl. *Proc. Natl. Acad. Sci.* **2020**, *117* (4), 1941–1950.
584 <https://doi.org/10.1073/pnas.1905232116>.
- 585 (54) GBD 2019 Diseases and Injuries Collaborators. Global Burden of 369 Diseases and Injuries
586 in 204 Countries and Territories, 1990–2019: A Systematic Analysis for the Global Burden
587 of Disease Study 2019. *The Lancet* **2020**, *396* (10258), 1204–1222. <https://doi.org/Global>
588 [burden of 369 diseases and injuries in 204 countries and territories, 1990–2019: a](https://doi.org/Global)
589 [systematic analysis for the Global Burden of Disease Study 2019.](https://doi.org/Global)
- 590 (55) Rodriguez, A.; Brickley, E.; Rodrigues, L.; Normansell, R. A.; Barreto, M.; Cooper, P. J.
591 Urbanisation and Asthma in Low-Income and Middle-Income Countries: A Systematic

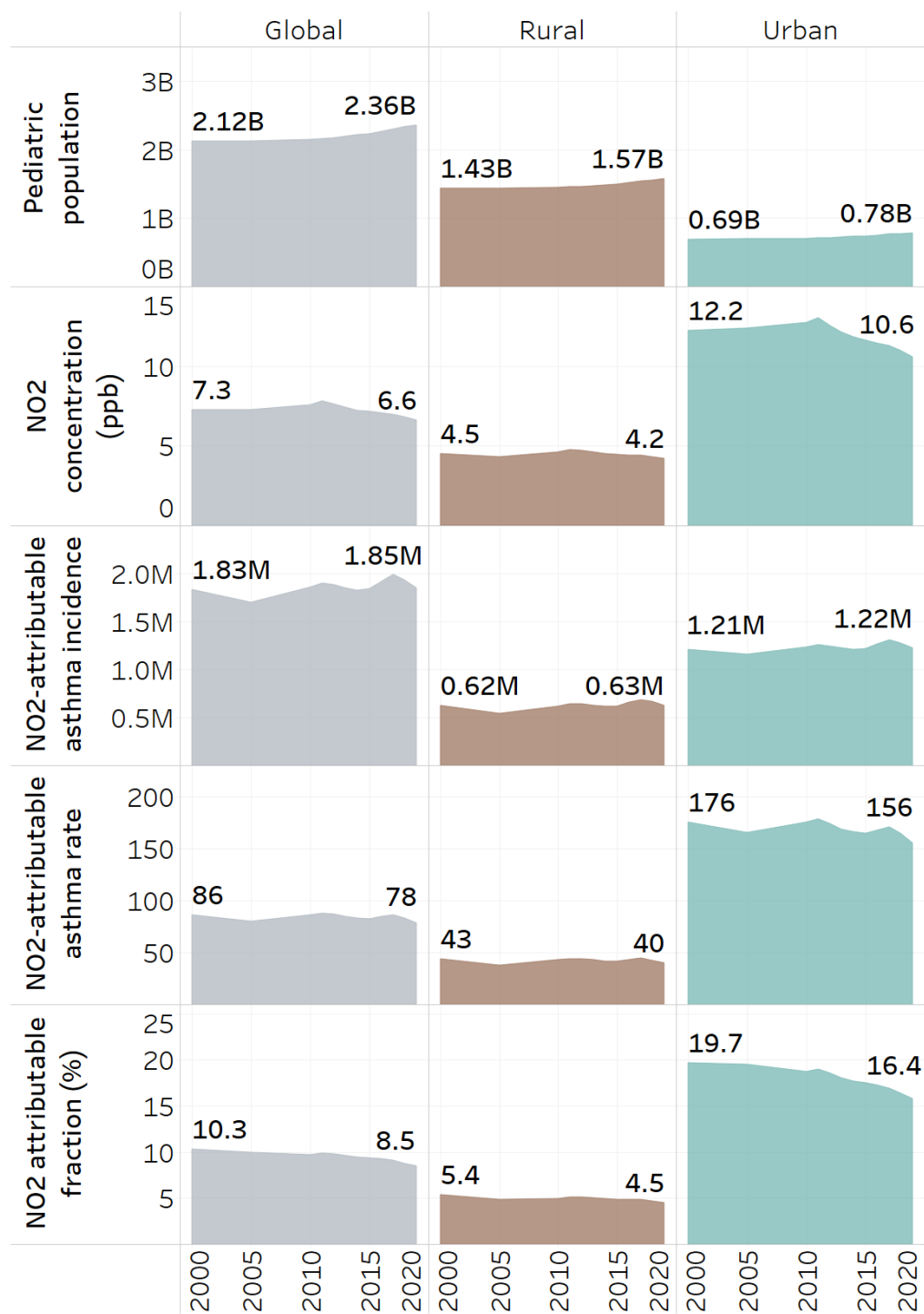
592 Review of the Urban–Rural Differences in Asthma Prevalence. *Thorax* **2019**, *74* (11),
593 1020–1030. <https://doi.org/10.1136/thoraxjnl-2018-211793>.
594 (56) Keet, C. A.; Matsui, E. C.; McCormack, M. C.; Peng, R. D. Urban Residence,
595 Neighborhood Poverty, Race/Ethnicity, and Asthma Morbidity among Children on
596 Medicaid. *J. Allergy Clin. Immunol.* **2017**, *140* (3), 822–827.
597 <https://doi.org/10.1016/j.jaci.2017.01.036>.
598
599



601

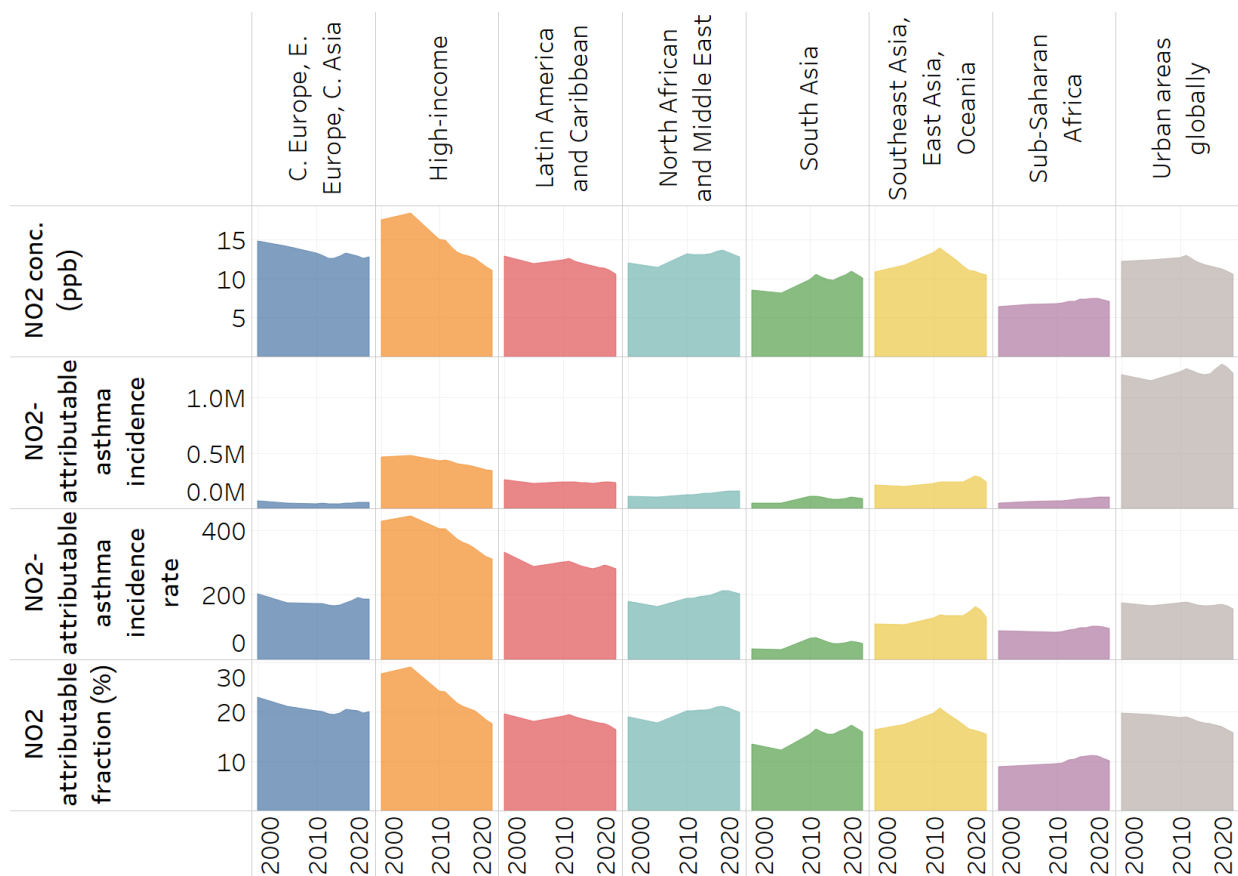
602 Figure 1. Annual average NO₂ concentrations at 1km x 1km resolution in a) 1990, 2000, 2010
603 and 2019 and b) difference between 2019 and 2000.

604



605

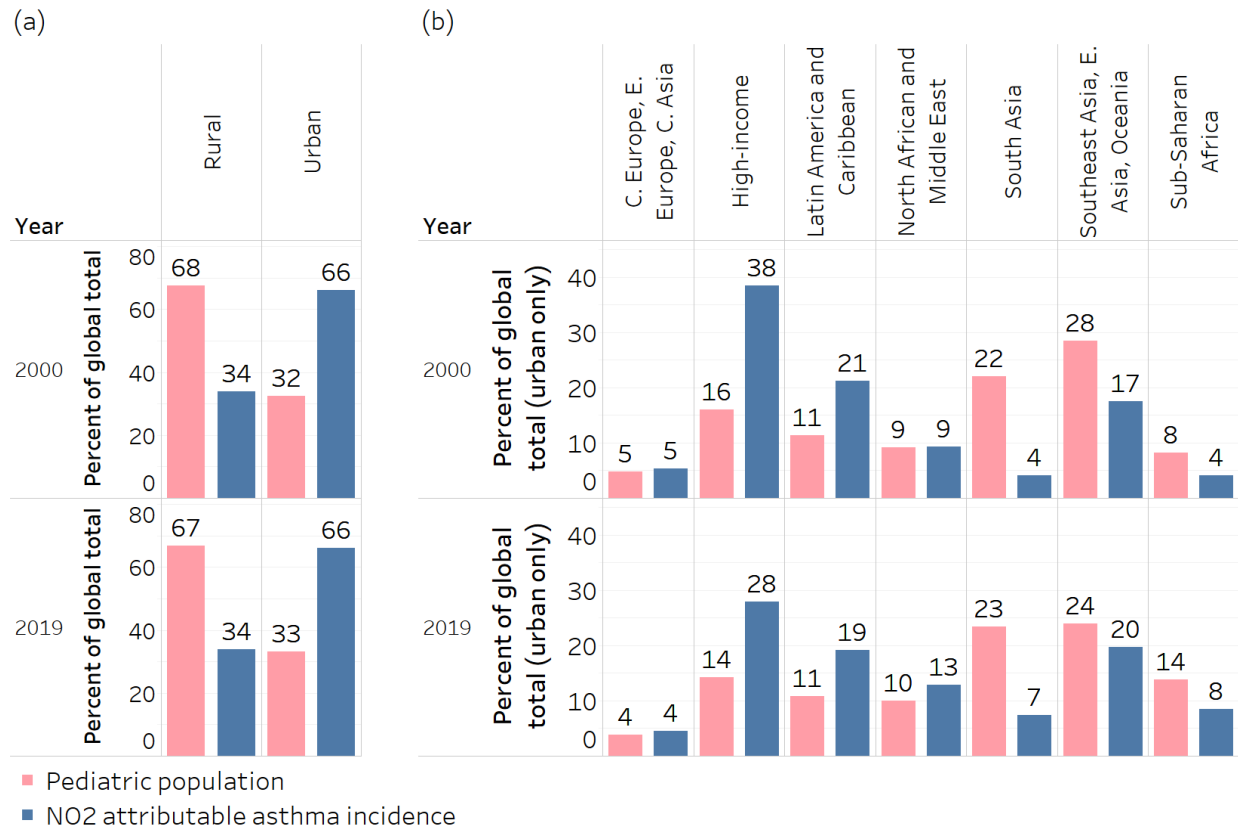
606 Figure 2. Trends (2000-2019) in population-weighted annual average NO₂ concentrations (ppb),
 607 NO₂-attributable pediatric asthma incidence, NO₂-attributable pediatric asthma incidence rate
 608 (per 100,000 children), and NO₂ attributable fraction globally (%), in all rural areas, and in
 609 13,189 urban areas. Uncertainty intervals for NO₂-attributable pediatric asthma incidence are not
 610 shown since they are based on error in the relative risk estimate, which is constant over time.



612

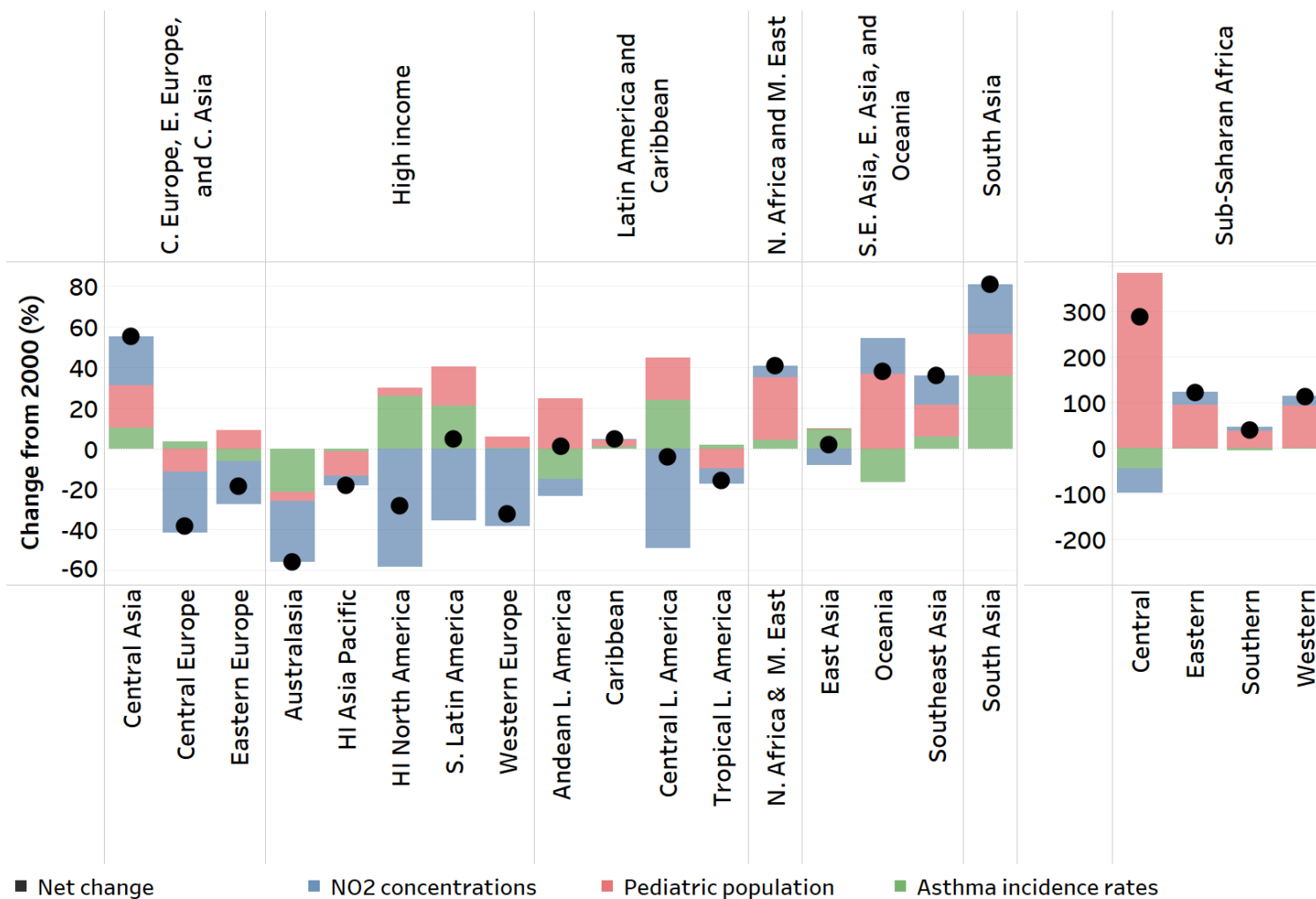
613 Figure 3. Trends (2000-2019) in population-weighted annual average NO₂ concentrations (ppb),
 614 NO₂-attributable pediatric asthma incidence (cases), NO₂-attributable pediatric asthma rates (per
 615 100,000 children), and NO₂ attributable fraction (% of all pediatric asthma incidence) in urban
 616 areas in each sub-region. Results for each subregion within each super-region are shown in
 617 Figure S8. Uncertainty intervals for NO₂-attributable pediatric asthma incidence are not shown
 618 since they are based on error in the relative risk estimate, which is constant over time.

619



620

621 Figure 4. Percent of global total pediatric population and NO₂-attributable asthma cases in 2000
 622 and 2019, for a) all rural areas and 13,189 urban areas globally, and b) urban areas within each
 623 region.



624

625 Figure 5. Contribution of pediatric population, baseline pediatric asthma rates, and NO₂ concentrations to changes in estimated NO₂-
 626 attributable pediatric asthma incidence between 2000 and 2019 for each sub-region. A different y-axis is used for regions in Sub-
 627 Saharan Africa. Results for the full time period are shown in Figure S11.

Supplemental material:

Long-term trends in urban NO₂ concentrations and associated pediatric asthma incidence: estimates from global datasets

Susan C. Anenberg, Arash Mohegh, Daniel L. Goldberg, Gaige H. Kerr, Michael Brauer, Katrin Burkart, Perry Hystad, Andrew Larkin, Sarah Wozniak, Lok Lamsal

Methods for adjusting surface NO₂ concentrations in rural areas

For grid cells >5km away from roadways and in rural areas, we developed new NO₂ concentration estimates using NO₂ column observations from the OMI satellite instrument with some adjustments to fill spatial and temporal gaps in the OMI satellite record, and to estimate 24-hour averages from the early afternoon OMI overpass time (Figure S1). We use an OMI NO₂ version 3, level 4 surface concentration dataset (0.1° x 0.1° resolution) for 2011, which followed methods described by Lamsal et al.¹ and was obtained from the NASA Goddard Space Flight Center (GSFC). The newer version 4 OMI retrieval uses enhanced surface reflectivities in the calculation of the tropospheric column amounts, but surface concentrations prepared by NASA GSFC are not currently available from the version 4 product. Due to the lack of satellite dataset coverage over snow/ice covered areas, some gridcells (mostly in higher latitudes) have no OMI observations in some months. We used the MERRA-2 reanalysis product (0.625° x 0.5° resolution) to generate a correction factor to ensure availability of NO₂ concentrations in all locations and months, as follows:

$$\text{Equation S1: } \textit{Correction factor\#1} = \frac{\textit{MERRA2}_{\textit{annual average}}}{\textit{MERRA2}_{\textit{average for same months that OMI level 4 is available}}}$$

We also applied a second correction factor to convert surface NO₂ concentrations from the early afternoon OMI overpass time (13:00 local time) to 24-hour averages. Following Anenberg et al.², we used NO₂ surface concentrations from the GMI-Replay chemical transport model^{3,4} (2° x 2.5° resolution) simulations to generate these correction factors, as follows:

$$\text{Equation S2: } \textit{Correction factor\#2} = \frac{\textit{GMI}_{\textit{24 hour average}}}{\textit{GMI}_{\textit{13:00}}}$$

The NO₂ surface concentration estimates used for gridcells >5km away from roads and in rural areas were then generated using the following formula:

$$\text{Equation S3: } \textit{Adjusted rural concentrations} = \textit{OMI level 4} \times \textit{Correction factor\#1} \times \textit{Correction factor \#2}$$

For rural gridcells within 5km of major roadways, we linearly scaled between Larkin et al.⁵ values and the new adjusted rural concentrations in the span of the 5 km distance. The result of these steps is a 1km x 1km annual average surface NO₂ concentration dataset for 2011 that uses Larkin et al.⁵ values in gridcells that are categorized as urban or over roads, and a new concentration dataset derived from OMI satellite observations in rural areas (Figure S2).

Methods for scaling NO₂ concentrations from 2011 to 1990-2019

The GBD requires NO₂ concentrations for each year included in the comparative risk assessment, from 1990-2019. We therefore scaled the new 2011 surface NO₂ concentration dataset to each year in this time period, in five-year

increments from 1990-2005, and annually from 2010-2019. For the years 2005-2019, we scaled surface NO₂ concentrations from 2011 to each year using 3-year rolling averages of annual average NO₂ columns from the OMI version 4.0 level 2 product (13 km x 25 km resolution at nadir; Figure S3) at the gridcell level. We use NO₂ columns because surface concentrations derived from the version 4 OMI retrieval are not yet available. We oversampled the column NO₂ dataset to 0.1° x 0.1° resolution and re-gridded to 0.0083° x 0.0083° (approximately 1km x 1km). The 3-year rolling averages remove noise from the satellite data. For 2005 and 2019, we did not have data to create 3-year rolling averages, so we used that year's NO₂ columns directly. The years 1990, 1995, and 2000 predated the OMI observational record. We therefore used NO₂ concentrations from the MERRA-2 reanalysis product to scale 2011 NO₂ concentrations to those years.⁶ To remove model noise, we created the MERRA-2 scaling factors across broad world regions (Figure S5), as opposed to applying scaling factors on a gridcell by gridcell basis as we did for the OMI scaling.

The final result used for estimating the global burden of disease from NO₂ is a global, 0.0083° x 0.0083° (approximately 1km x 1km) resolution dataset of annual average surface NO₂ concentrations from 1990-2019 (Figure 1).

Evaluation of NO₂ concentration dataset

The Larkin et al.⁵ NO₂ concentration dataset was evaluated extensively in that work and agreed well with ground observations in urban areas. Here we add two limited new analyses to evaluate the changes we made in rural areas and the scaling other years (focusing specifically on the latest year, 2019).

We evaluated the rural NO₂ concentration estimates using the European Monitoring and Evaluation Program (EMEP) ground monitoring dataset, which has a large number of stations in rural areas (Table S1 and Figure S6). Other ground monitoring datasets (e.g. from EPA) may have rural sites, but we found that most were located directly downwind from urban areas. For example, the average surface annual mean NO₂ concentration in rural areas in 2011 from the EPA network is 4.3 ppb, likely too high to represent true background concentrations. We aggregated the available monitoring stations for the year 2011 to calculate annual averages and used a set of criteria to filter for stations that mostly closely represent background concentrations: 1) Stations with >300 days of data (the threshold was selected based on the distribution in days available for stations); 2) Stations that are at least 500m away from roads; 3) Stations that are not in urban and suburban areas. After applying these criteria, 67 stations across Europe remained. The evaluation is performed based on the aggregated annual average surface NO₂ concentrations for each monitor, and the value of the gridcell corresponding to that monitor for both original exposure dataset and final product.

The evaluation results show that the newly developed NO₂ surface concentrations outperformed the Larkin et al.⁵ concentrations in rural areas, based on Root Mean Squared Error (RMSE), Mean Absolute Error (MAE), Mean Bias (MB), and correlation with ground observations (Table S1). The slope of the best fitted line is improved from 1.41 to 1.10, and the mean ratio of estimated to observed concentrations is improved from 1.81 to 1.32 (Table S1 and Figure S6). The RMSE is reduced from 3.37 ppb to 2.26 ppb, and MAE is improved from 2.74 ppb to 1.72 ppb, and the MB is reduced from 2.40 ppb to 1.02 ppb. The correlation between the estimated surface concentrations and ground measurements is improved from Pearson correlation coefficient (R) of 0.51 in the original product to 0.58.

In addition to the comparison of our dataset with previously published NO₂ concentrations during their overlapping time period, we further test the fidelity of our dataset for a more recent year (Figure S7). We obtain annual average observations for 2019 from three different networks: the National Air Pollution Surveillance (NAPS) program in Canada⁷, the Air Quality System (AQS) in the United States⁸, and the European Environment Agency (EEA) in Europe.⁹ These networks provide data from 4,348 individual monitors (181 NAPS, 466 AQS, and 3,701 EEA), and we compare each monitor's NO₂ concentration to the concentration in the gridcell co-located with each monitor for

2019. All monitor data for 2019 have passed several quality control tests and quality assurance assessments by the entities that disseminate these data.

The mean bias (normalized mean bias) was -2.27 ppb (-20.40%) in Europe, 1.69 ppb in the U.S. (20.79%), and 3.34 ppb (49.56%) in Canada across the three networks in 2019 (Figure S7b,e,h). In urban areas specifically, the mean bias was -2.87 (-22.51%) in Europe, 1.26 ppb (12.21%) in the U.S., and 3.93 ppb (50.14%) in Canada for an average of 0.77 ppb across these three networks (Figure S7c,f,i). The mean bias at rural sites averaged over the three networks is 1.56 ppb, similar in magnitude to the rural bias reported for 2010-2012 (compare Figure S7c,f,i with Table S1).

The high mean bias evident in the NAPS and AQS datasets (Figure S7b-c, e-f) could, in part, reflect known issues with NO₂ monitors, which have been reported to overestimate NO₂ concentrations by up to ~50% due to interference from reactive nitrogen compounds, especially at locations distant from NO_x sources.¹⁰ Additionally, this high bias could also stem from monitors sited near traffic or other sources of NO_x emissions that may not be resolved in our ~1 km² dataset.

The paucity of monitors throughout large swaths of Canada and the United States (Figure S7a, d) and throughout the rest of the world inhibits a more in-depth performance assessment of our dataset and highlights the urgent need for more strategic and equitable monitoring of ambient air pollution (e.g. ¹¹).

Methods for decomposing parameter contributions to NO₂-attributable asthma trends

We calculate the contribution of each parameter used in health impact assessment (population, baseline asthma rates, and concentrations) using four sets of simulations:

- Control scenario, where we calculated the asthma cases for each year.
- Three “parameter rollback” simulations in which we revert one of the parameters (population, baseline asthma rates, or concentrations) to the base year 2000.

By comparing each of the three parameter rollback scenarios to the control scenario, we calculate the contribution of each parameter to the change in asthma cases between 2000 and all other years. We use the following set of equations to calculate the contribution of each parameter.

We use Equation S4 to calculate pediatric asthma incidence attributable to NO₂ for the control scenario. This equation is the same as Equation 1 in the main text, but we denote the parameters differently here to make it easier to compare with the control scenario equations.

$$\text{Equation S4: } \text{Control}_t(x_t, y_t, z_t) = x_t \times y_t \times z_t$$

Where Control_t is the NO₂-attributable pediatric asthma incidence for year t , x_t is the baseline pediatric asthma rate for year t , y_t is the pediatric population for year t , and z_t is the fraction of pediatric asthma incidence that is attributable to NO₂ for year t .

We then calculate NO₂-attributable pediatric asthma incidence for each simulation, replacing one parameter with its value in the year 2000 while holding the other two parameters at the same value used in the control scenario (Equations S5-S7).

$$\text{Equation S5: } \text{Simulation}_{x,t}(x_0, y_t, z_t) = x_0 \times y_t \times z_t$$

Equation S6: $Simulation_{y,t}(x_t, y_0, z_t) = x_t \times y_0 \times z_t$

Equation S7: $Simulation_{z,t}(x_t, y_t, z_0) = x_t \times y_t \times z_0$

Where $Simulation_{i,t}$ is the estimated NO₂-attributable pediatric asthma incidence for year t, where we have reverted one parameter back to the base year of 2000.

We then calculate the ratio of estimated NO₂-attributable pediatric asthma incidence in the control scenario versus in each of the parameter rollback scenarios, as shown in Equation S8.

Equation S8: $Ratio_{i,t} = \frac{Control_t}{Simulation_{i,t}}$

Since NO₂-attributable pediatric asthma incidence is calculated by multiplying three parameters, we assume that the ratio of NO₂-attributable asthma incidence between year t and base year 2000 would be equivalent to the multiplication of the three rollback scenario ratios calculated in Equations S5-S7 (Equation S9). In this step we assume that aggregating the three parameter rollbacks separately is equivalent to reverting all of them together.

Equation S9: $\frac{Asthma_t}{Asthma_0} \approx Ratio_{x,t} \times Ratio_{y,t} \times Ratio_{z,t}$

To calculate the contribution of each parameter individually, we need to transform the parameter ratios so that they add up to 1 when summed. We therefore calculate a logarithm in the base of the left side of Equation S9 ($Asthma_t/Asthma_0$); since the logarithm of every number in its own base equals 1, this step makes the left side equal to 1 (Equation S10).

Equation S10: $1 = \log(Ratio_{x,t}) + \log(Ratio_{y,t}) + \log(Ratio_{z,t})$

Finally, we multiply each of the three log-transformed parameter rollback ratios by the total percentage change in NO₂-attributable asthma incidence between years 2000 and t to calculate the percent contribution of each parameter to that total change (Equation S11).

Equation S11: $Contribution_{i,t} = \frac{Asthma_t}{Asthma_0} \times \log(Ratio_{i,t})$

Using this methodology, we calculated percent contributions for each of the three health impact function parameters (concentration, population, asthma rates) that add up to the total percentage changes between the two years, while remaining loyal to the multiplicative nature of the original health impact assessment function.

Supplemental Tables and Figures

Table S1. Statistical parameters for NO₂ concentrations from the Larkin et al.⁵ dataset and our new concentration estimates for rural areas compared with EMEP rural observations. Values reported here for Larkin et al.⁵ differ from those reported in their paper because here we are only evaluating predicted concentrations in rural areas at the EMEP monitor locations.

	Root Mean Square Error (RMSE) (ppb)	Mean Absolute Error (MAE) (ppb)	Mean Bias (MB) (ppb)	Pearson coefficient (R)	Mean ratio: Estimate/obs	Slope of best fitted line
New product	2.26	1.72	1.02	0.58	1.32	1.10
Larkin et al. ⁵	3.37	2.74	2.40	0.51	1.81	1.41

Table S2. Count of urban clusters in each GBD region/super region. The total does not match the total urban clusters in analysis (13,189) since some urban clusters are located at the border between two regions.

Super region name	Region name	Count
Central Europe, Eastern Europe, and Central Asia		628
	Central Asia	148
	Central Europe	161
	Eastern Europe	319
High-income		1280
	Australasia	35
	High-income Asia Pacific	148
	High-income North America	389
	Southern Latin America	115
	Western Europe	593
Latin America and Caribbean		968
	Andean Latin America	93
	Caribbean	75
	Central Latin America	438
	Tropical Latin America	362
North Africa and Middle East		1231
	North Africa and Middle East	1231
South Asia		3899
	South Asia	3899
Southeast Asia, East Asia, and Oceania		2904
	East Asia	1955
	Oceania	49
	Southeast Asia	900
Sub-Saharan Africa		2313
	Central Sub-Saharan Africa	250
	Eastern Sub-Saharan Africa	1024
	Southern Sub-Saharan Africa	124
	Western Sub-Saharan Africa	915
Grand Total		13223

Table S3. Population-weighted NO₂ concentrations (ppb), NO₂-attributable pediatric asthma incidence (95% uncertainty interval in parentheses), NO₂-attributable pediatric asthma incidence rate (per 100,000), and NO₂ attributable fraction (%) for each super-region in 2000, 2005, 2010, and 2019.

Super region	Year	Pop-wt NO ₂ concentration (ppb)	NO ₂ -attributable pediatric asthma incidence	NO ₂ -attributable asthma rate (per 100,000)	NO ₂ attributable fraction
Central Europe, Eastern Europe, Central Asia	2000	15.1	65,000 (33,400 – 107,500)	202	23
	2010	13.6	44,300 (26,400 – 85,300)	172	20
	2019	12.7	54,900 (26,400 – 87,000)	188	20
High-income	2000	17.3	464,800 (264,700 – 725,800)	428	29
	2010	15.1	433,300 (255,500 – 655,000)	404	24
	2019	11.1	340,900 (191,400 – 523,200)	310	17
Latin America and Caribbean	2000	12.8	256,100 (147,300 – 397,000)	332	19
	2010	12.4	236,900 (138,000 – 380,300)	302	19
	2019	10.6	233,800 (125,300 – 375,800)	281	16
North Africa and Middle East	2000	12.1	111,800 (63,300 – 176,300)	180	19
	2010	13.2	120,100 (65,000 – 189,200)	189	20
	2019	12.8	157,600 (67,000 – 202,200)	203	20
South Asia	2000	8.6	50,000 (28,600 – 78,100)	33	13
	2010	9.9	106,500 (55,900 – 161,900)	65	15
	2019	10.1	90,400 (40,700 – 130,700)	50	16
Southeast Asia, East Asia, and Oceania	2000	11.1	211,300 (113,900 – 343,100)	109	16
	2010	14	226,600 (129,500 – 377,600)	128	18
	2019	10.6	240,900 (122,100 – 378,000)	129	15
Sub-Saharan Africa	2000	6.4	49,100 (27,400 – 78,700)	89	9
	2010	6.9	65,700 (26,000 – 74,700)	84	9
	2019	7.1	102,900 (30,200 – 90,900)	97	10

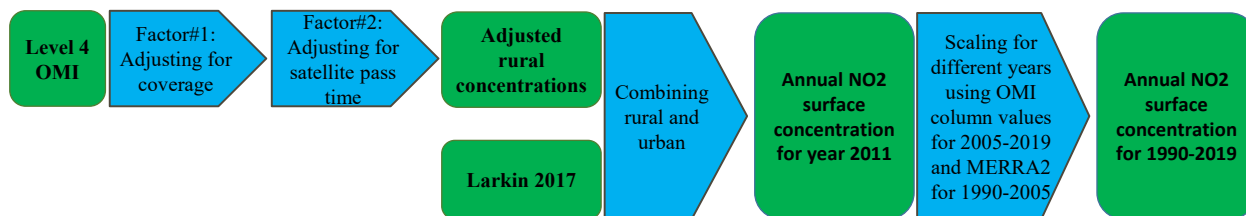


Figure S1. Schematic of datasets used and the process of combining them. Blue arrows represent applied processes.

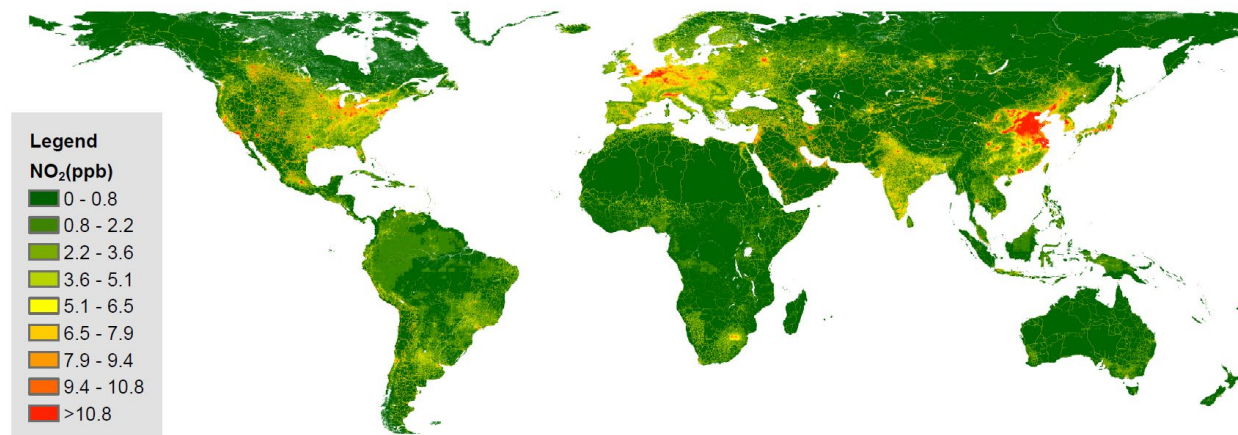


Figure S2. Annual average surface NO₂ concentration estimates for 2011 at ~1km x 1km resolution globally from this work, using a combination of Larkin et al.⁵ land use regression estimates, OMI satellite observations, and chemical transport modeling.

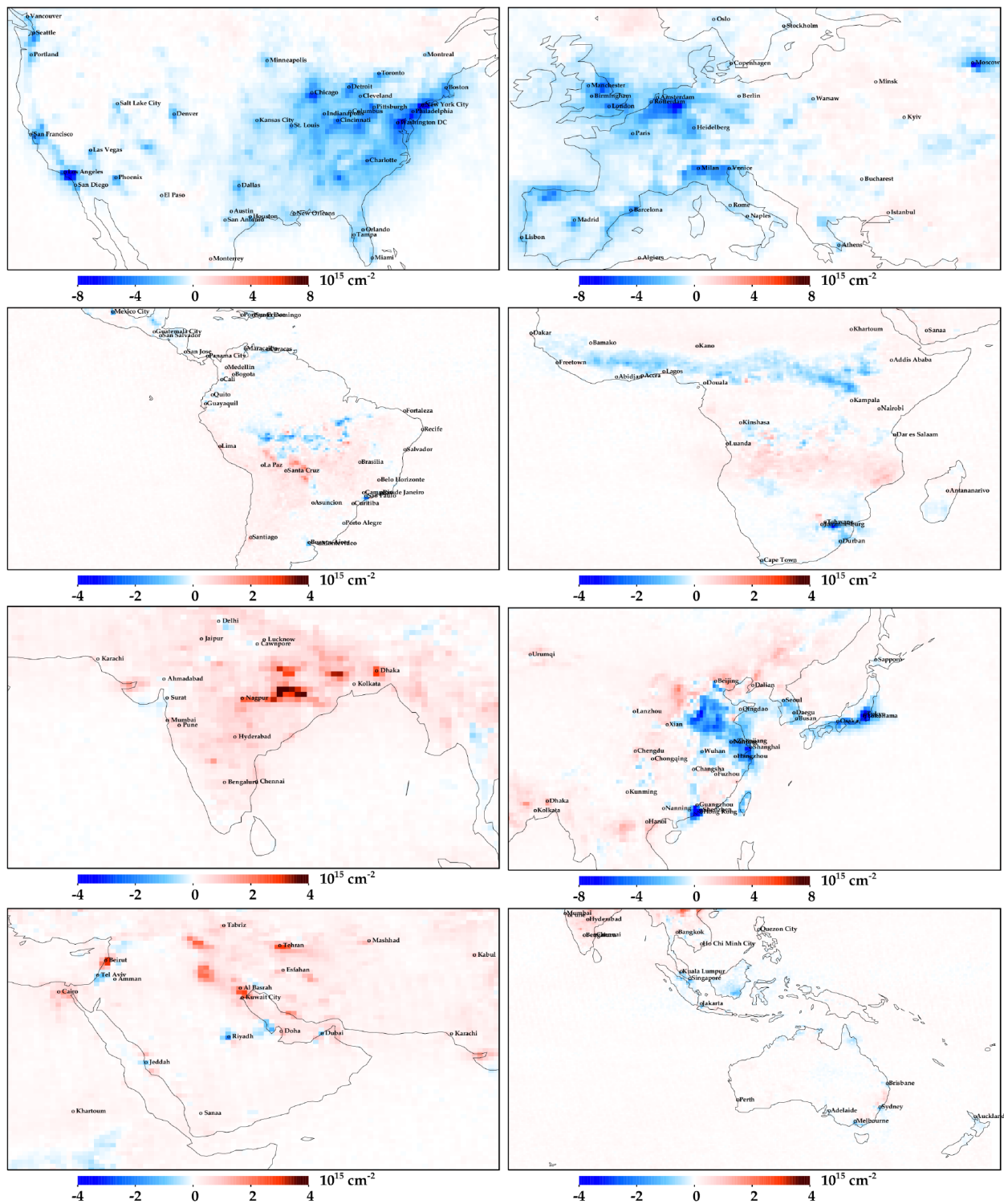


Figure S3. Regional trends in annual average NO₂ column densities ($0.5^\circ \times 0.5^\circ$) from the OMI satellite instrument (2005-2019).

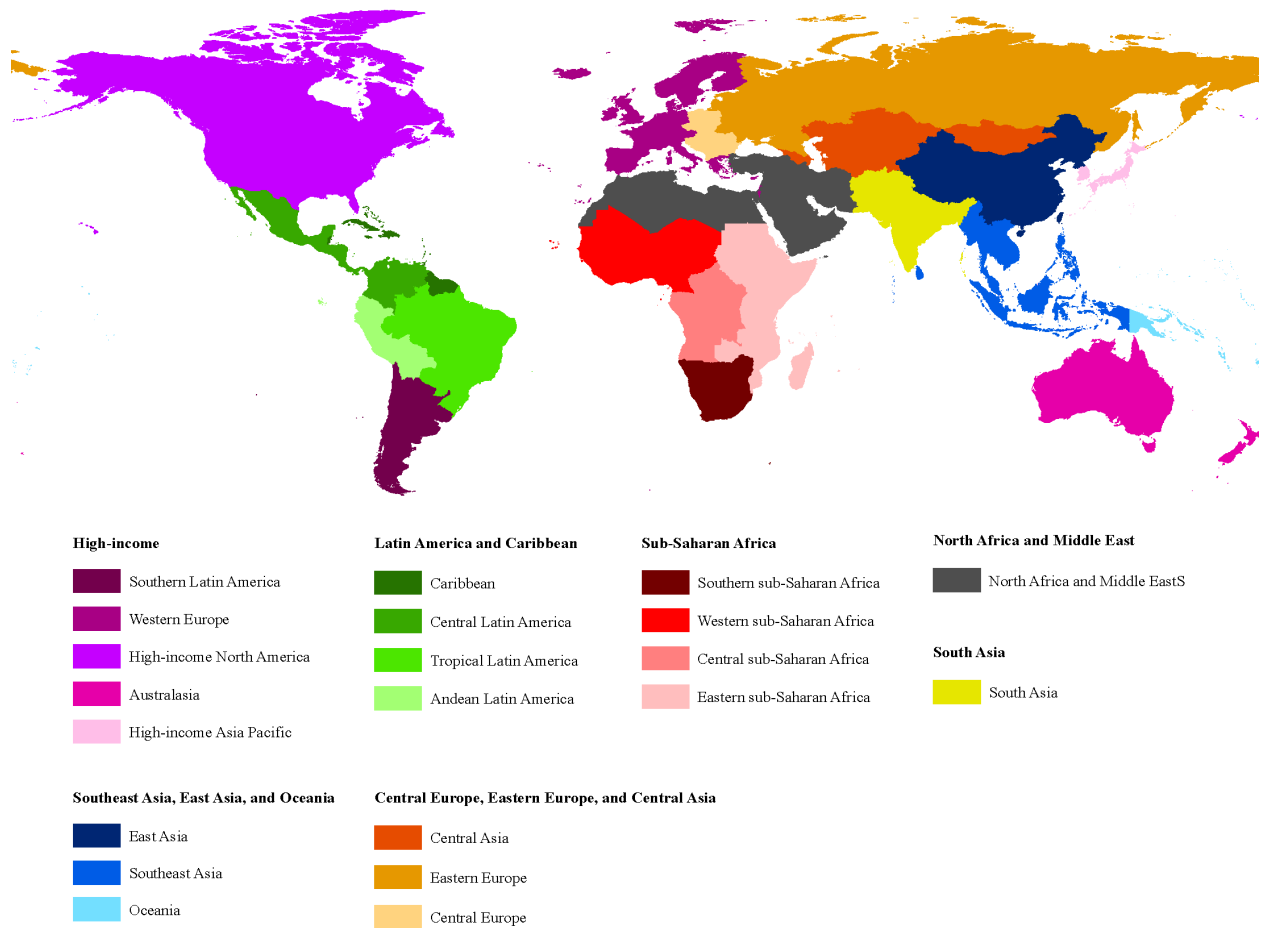


Figure S4. Countries and territories included in each region and super region, using regional definitions from the GBD 2019 Study.

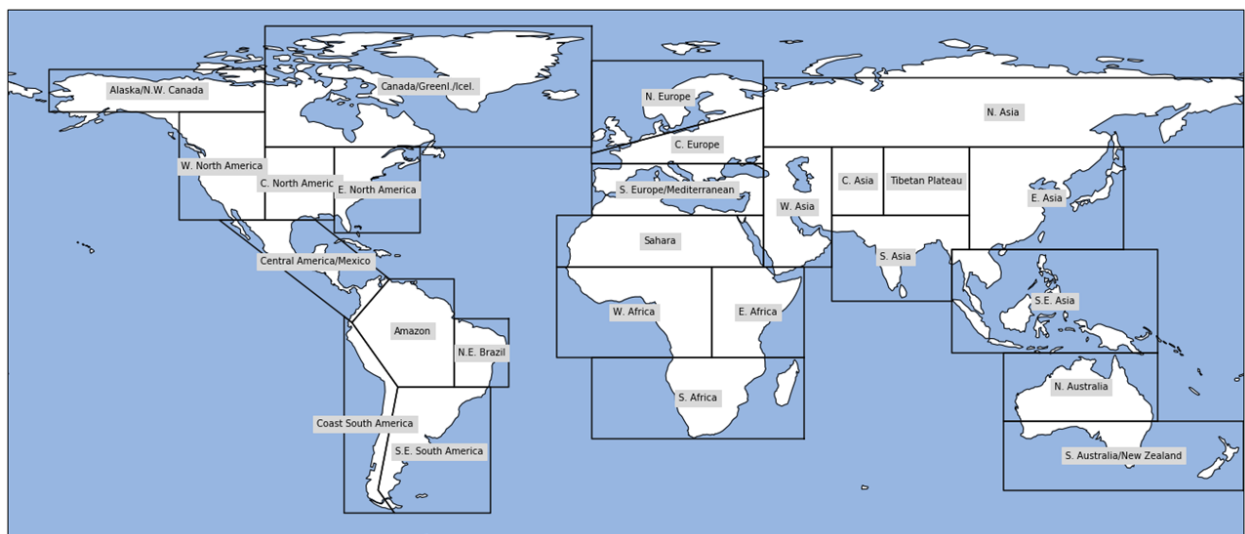


Figure S5. World regions used to generate the MERRA-2 scaling factors for NO₂ in 1990, 1995, and 2000.

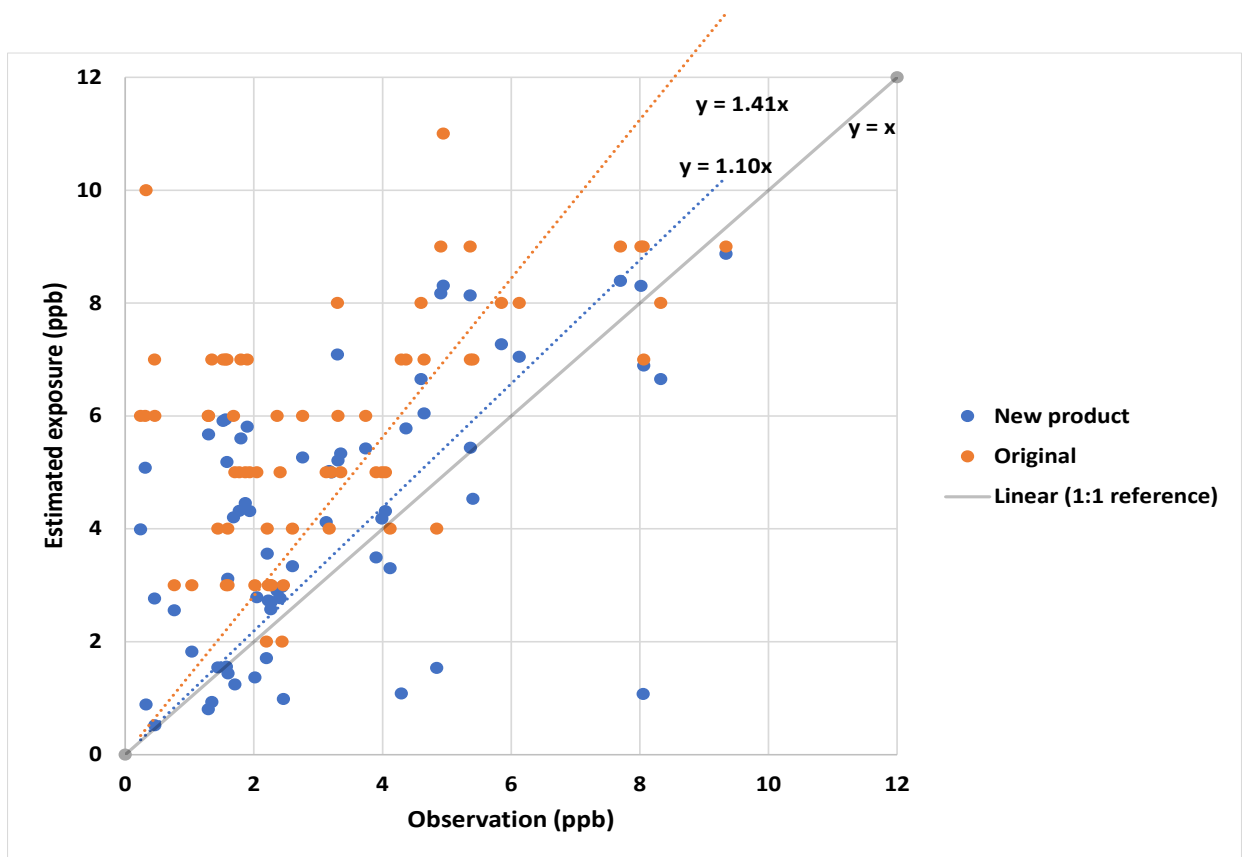


Figure S6. Comparison between annual average NO₂ concentrations from the original Larkin et al.⁵ product (orange) and our new NO₂ concentration product (blue), versus concentrations from ground measurements for 2011 in rural areas. A 1:1 reference line is added for comparison. Each point represents a monitor. Monitor data source: European Monitoring and Evaluation Programme (EMEP).

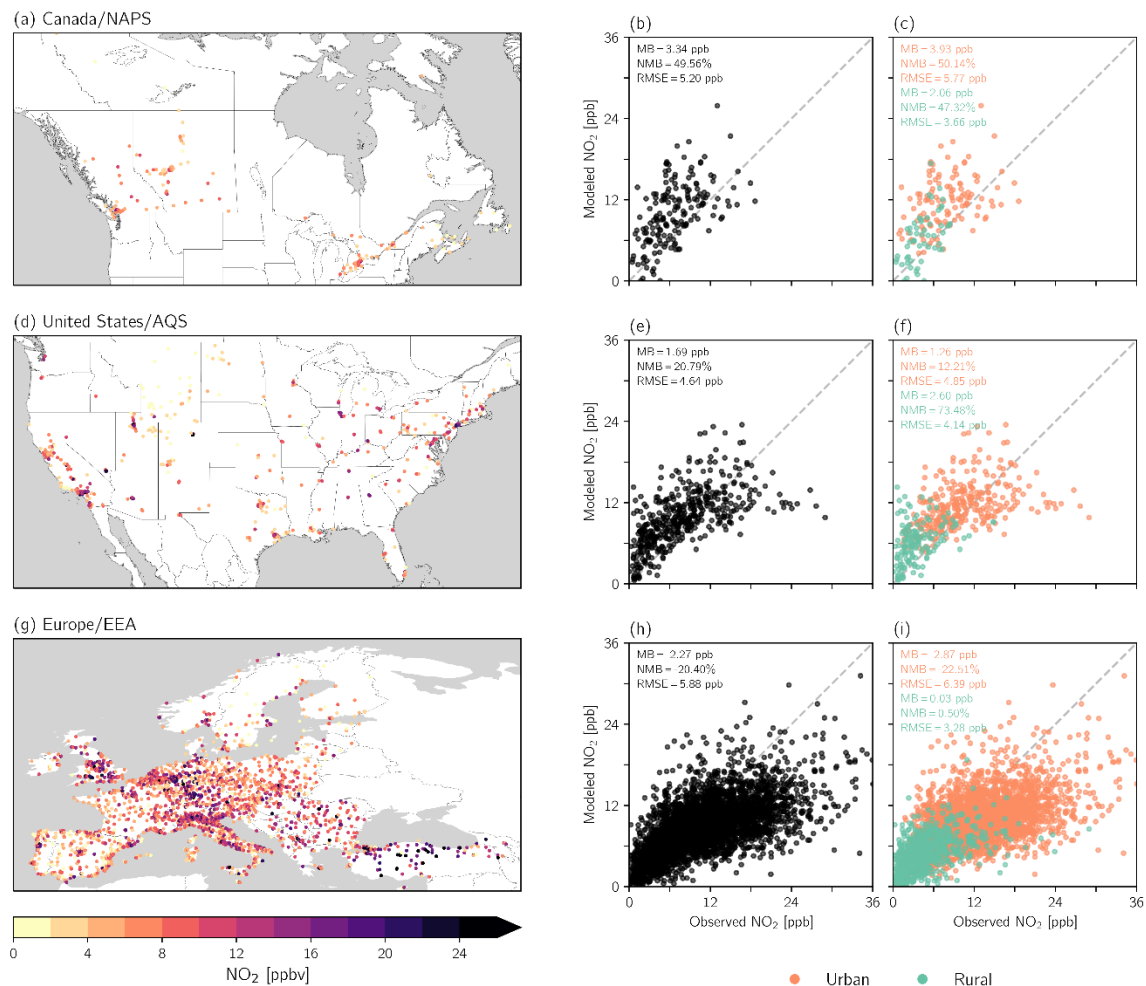


Figure S7. (a,d,g) The location of NO₂ monitors from the NAPS, AQS, and EEA networks and their annual average 2019 concentrations. (b,e,h) Annual average 2019 NO₂ concentrations from the gridcells co-located with each monitor versus the monitor concentrations. (c,f,i) are the same as (b,e,h) but for urban versus rural monitors. Rurality in (c,f,i) is determined with the GHS-SMOD dataset. The mean bias (MB; $= \bar{M} - \bar{O}$), normalized mean bias (NMB; $= (\frac{\bar{M}}{\bar{O}} - 1) \times 100\%$), and RMSE ($= \left[\frac{1}{N} \sum_{i=1}^N (M_i - O_i)^2 \right]^{\frac{1}{2}}$) are indicated in each scatterplot. Here, M corresponds to the new dataset and O corresponds to observed concentrations. A 1:1 reference line is included in scatterplots for comparison.

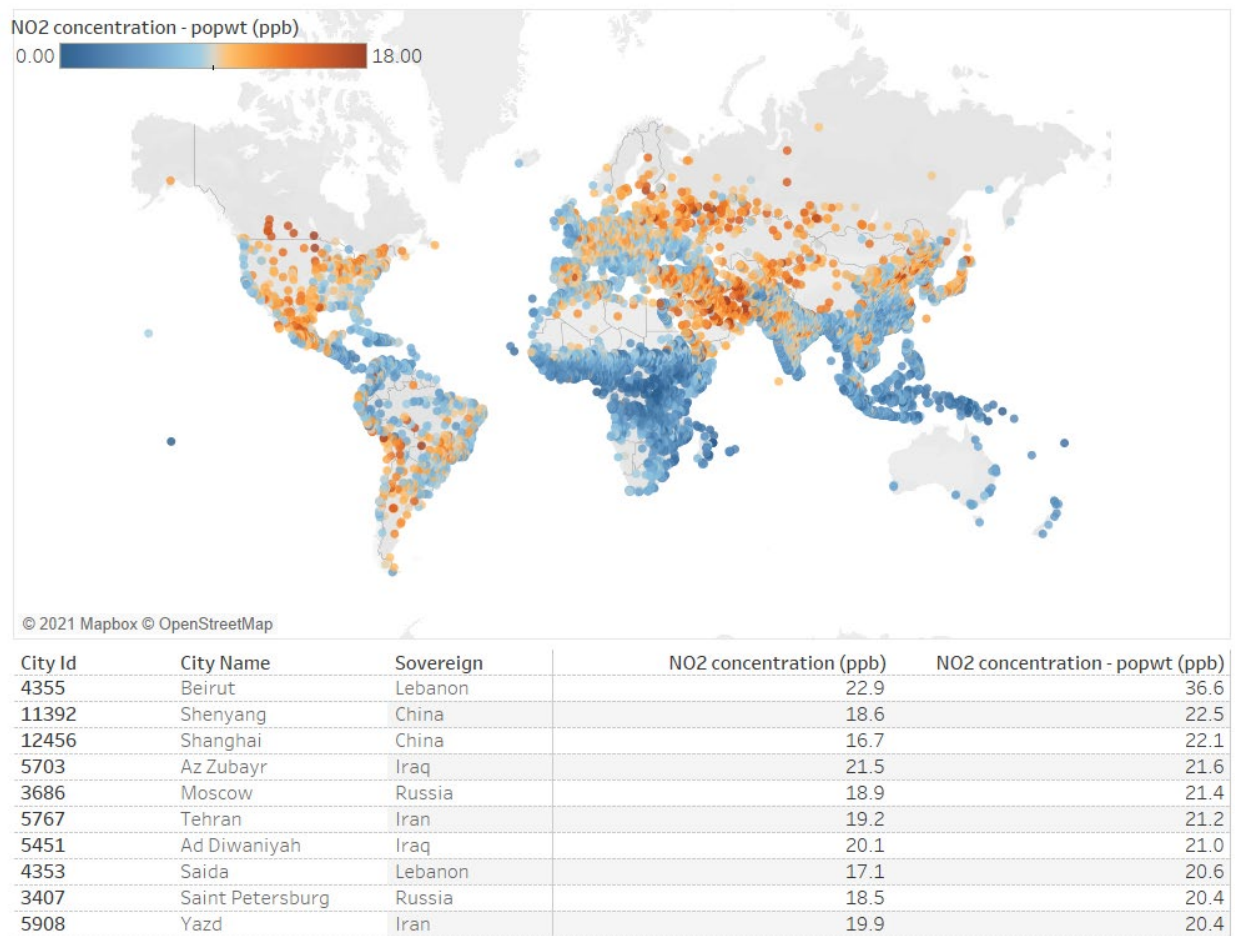


Figure S8. Population-weighted annual average NO₂ concentrations (ppb) for 13,189 urban areas (top) and the cities with the top 10 concentrations (bottom) in 2019. Color bar saturates at 18 ppb for greater contrast.

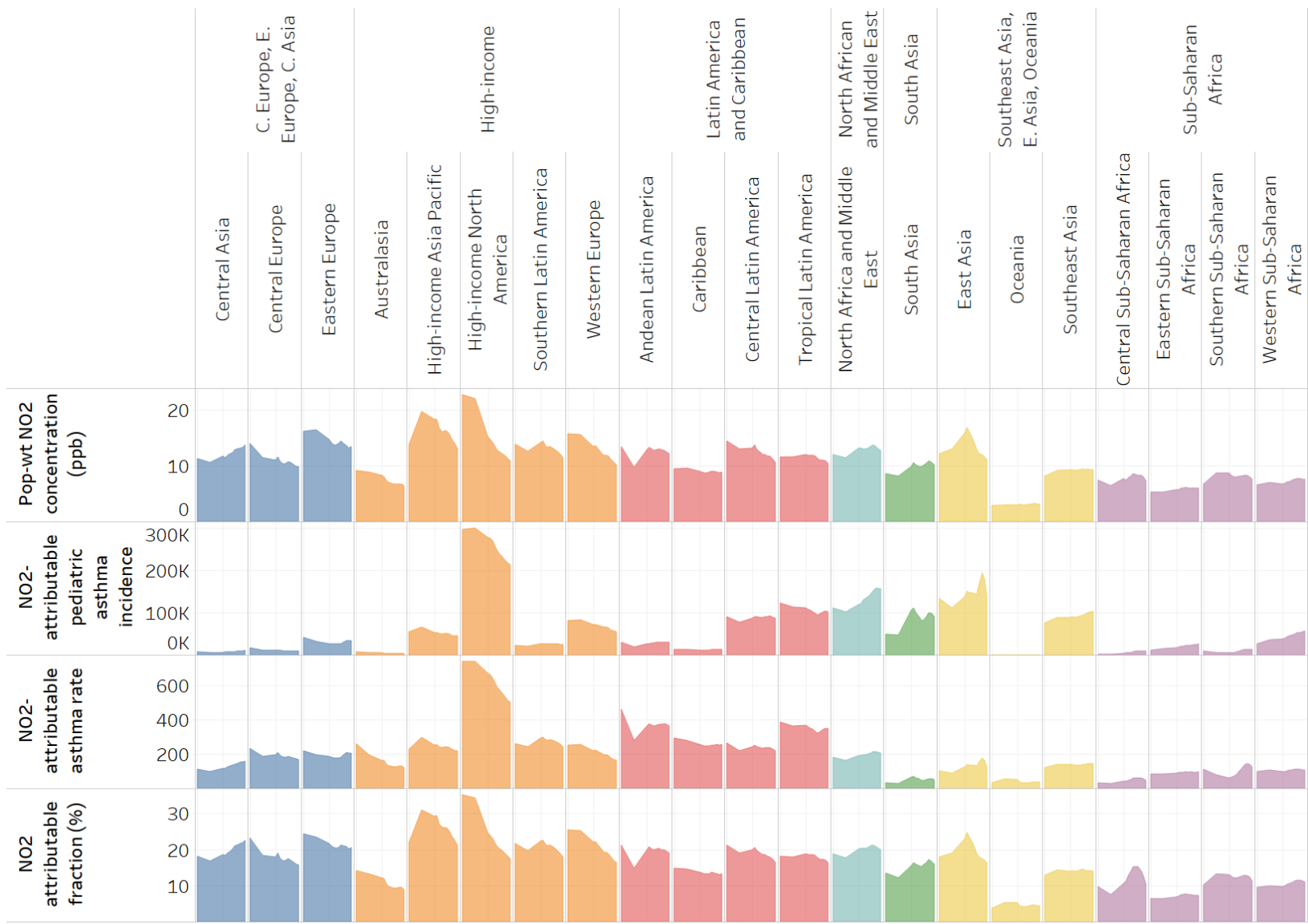


Figure S9. As for Figure 3, but for each subregion within each super-region.

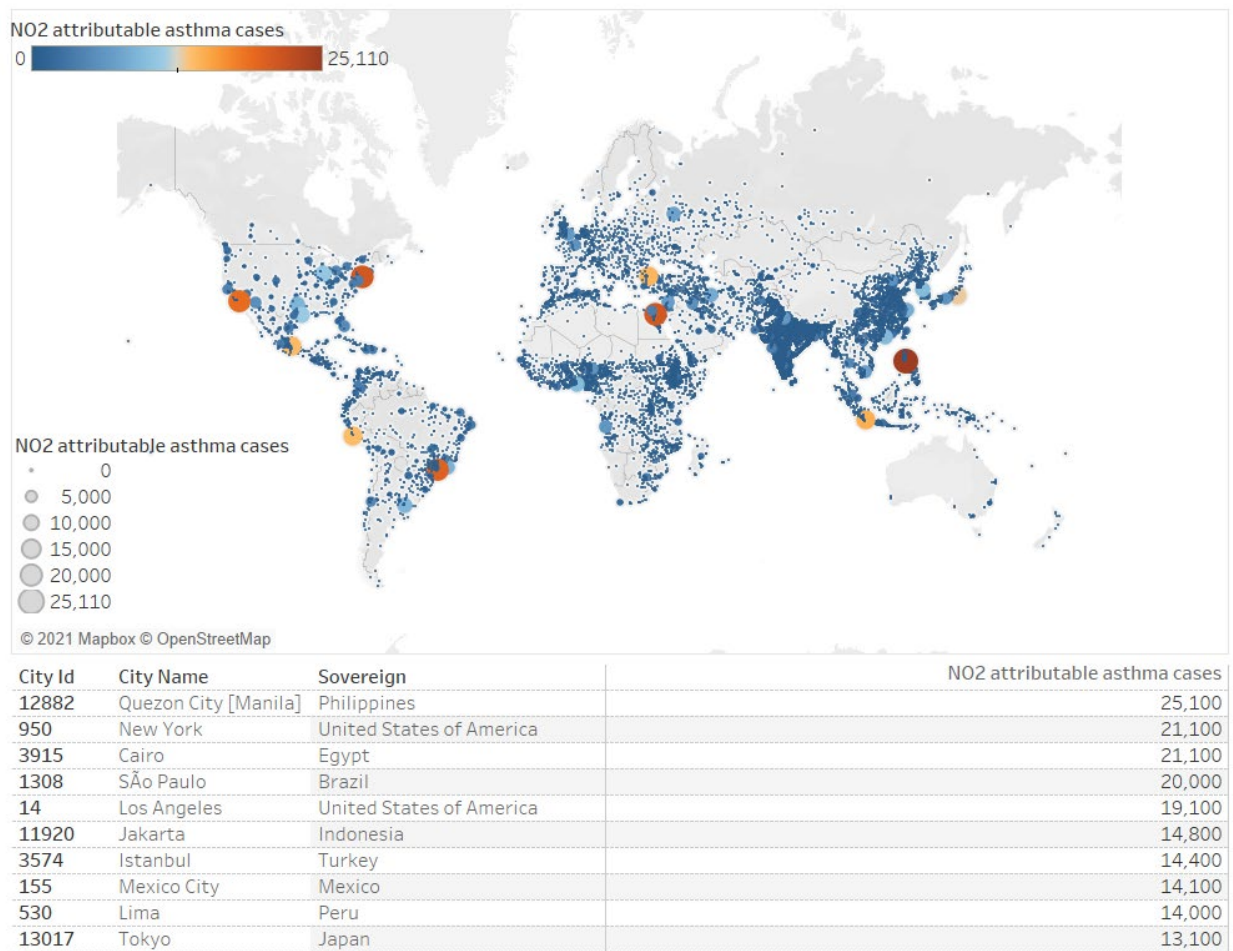


Figure S10. As for Figure S8, but for NO₂-attributable pediatric asthma incidence.

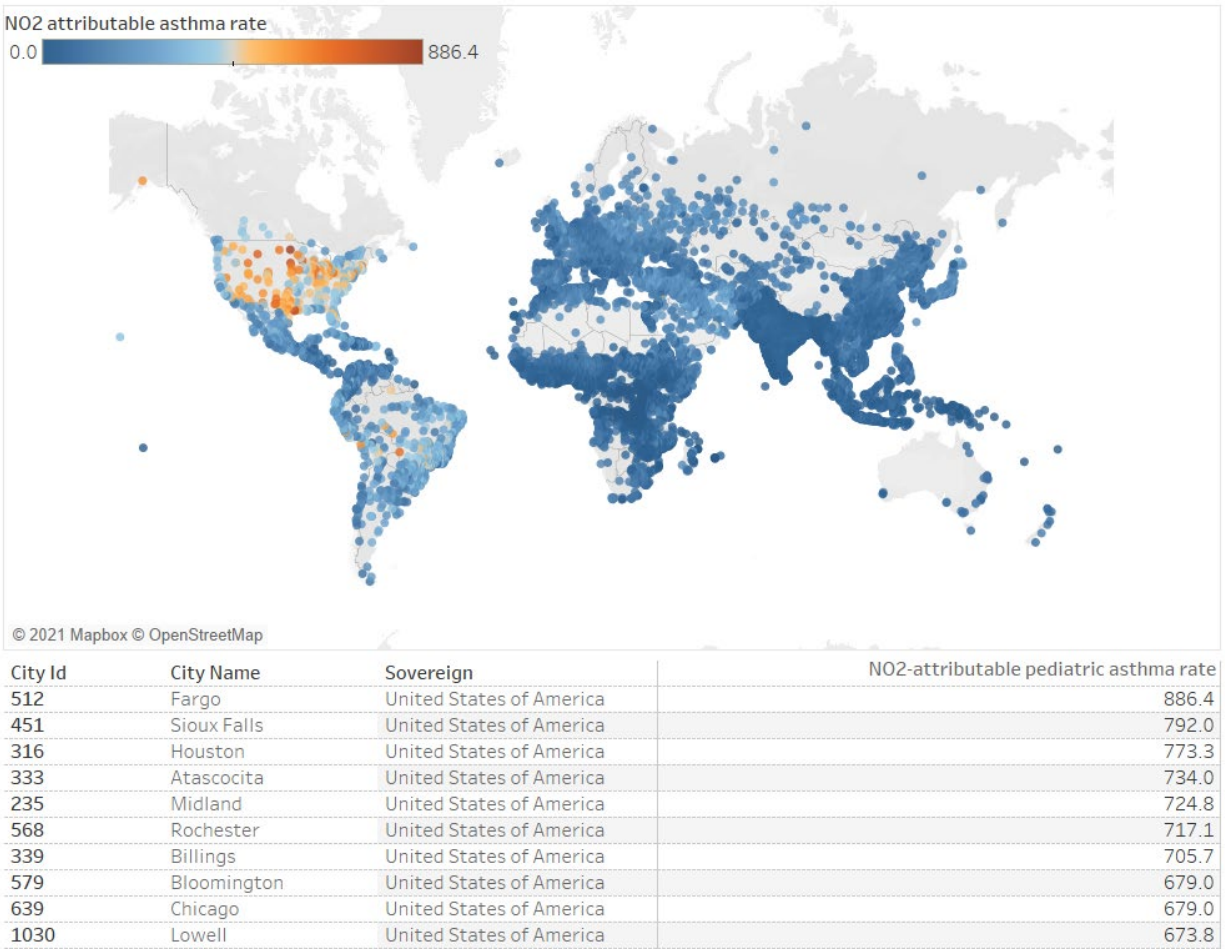


Figure S11. As for Figure S8, but for NO₂-attributable pediatric asthma incidence rate per 100,000 children.

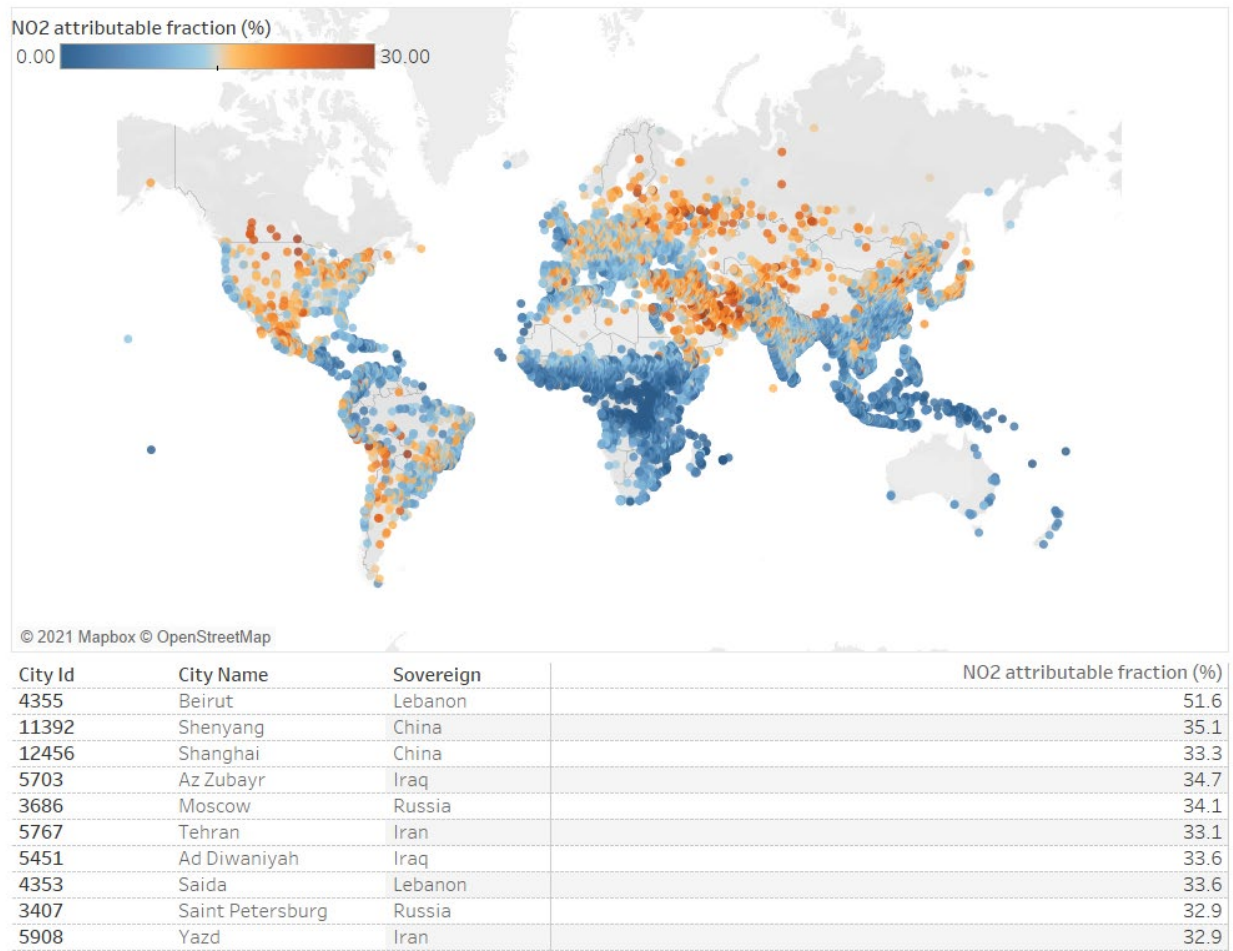


Figure S12. As for Figure S8, but for the fraction of pediatric asthma incidence attributable to NO₂ (%). Color bar saturates at 30% for greater contrast.

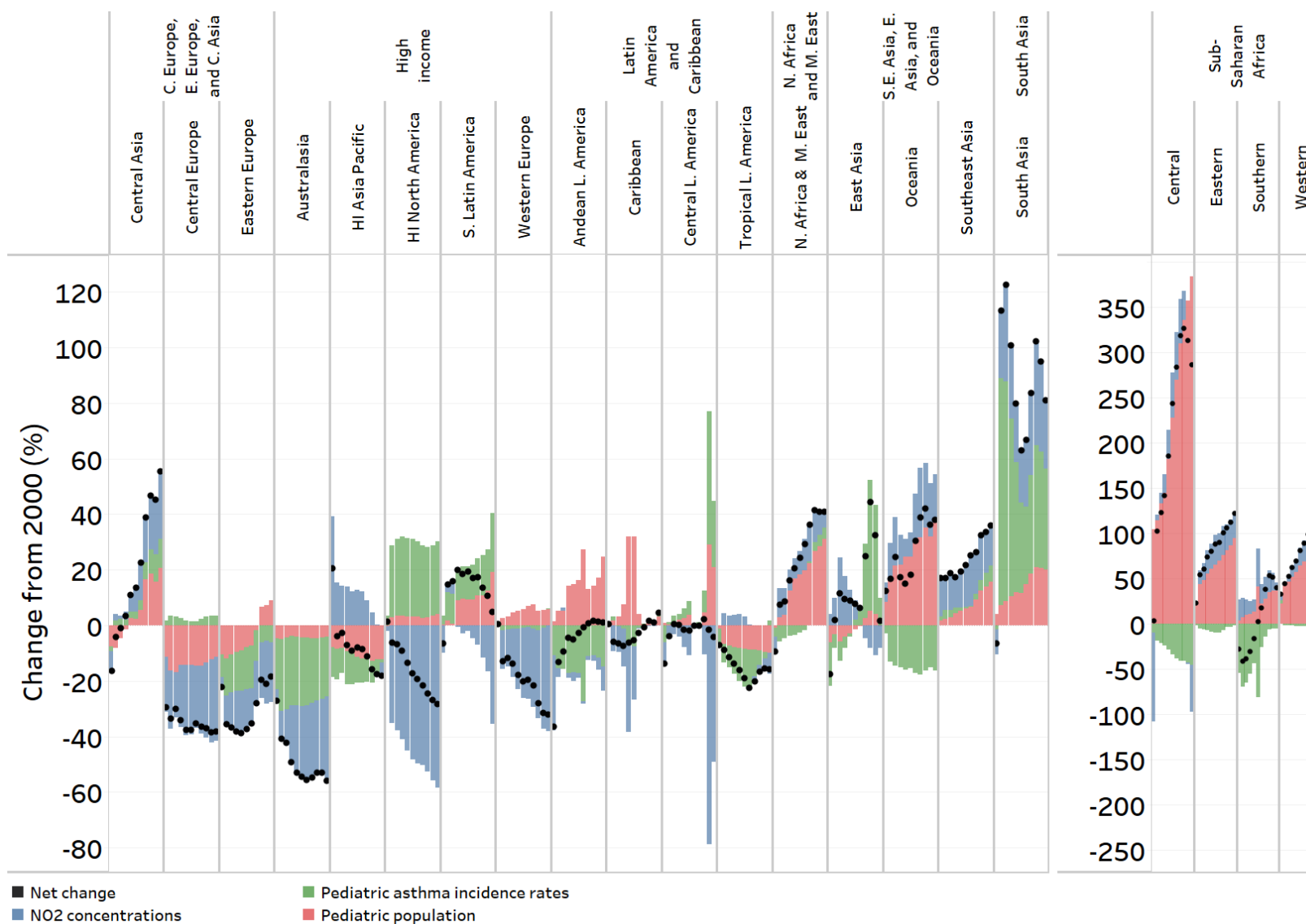


Figure S13. As for Figure 5, but for the change from 2000 to 2005 and 2010-2019 annually (represented left to right by the bars in each panel).

Supplemental References

- (1) Lamsal, L. N.; Martin, R. V.; van Donkelaar, A.; Steinbacher, M.; Celarier, E. A.; Bucsela, E.; Dunlea, E. J.; Pinto, J. P. Ground-Level Nitrogen Dioxide Concentrations Inferred from the Satellite-Borne Ozone Monitoring Instrument. *J. Geophys. Res.* **2008**, *113* (D16). <https://doi.org/10.1029/2007JD009235>.
- (2) Anenberg, S. C.; Henze, D. K.; Tinney, V.; Kinney, P. L.; Raich, W.; Fann, N.; Malley, C. S.; Roman, H.; Lamsal, L.; Duncan, B.; Martin, R. V.; van Donkelaar, A.; Brauer, M.; Doherty, R.; Jonson, J. E.; Davila, Y.; Sudo, K.; Kuylenstierna, J. C. I. Estimates of the Global Burden of Ambient PM_{2.5}, Ozone, and NO₂ on Asthma Incidence and Emergency Room Visits. *Environ. Health Perspect.* **2018**, *126* (10), 107004. <https://doi.org/10.1289/EHP3766>.
- (3) Strode, S. A.; Ziemke, J. R.; Oman, L. D.; Lamsal, L. N.; Olsen, M. A.; Liu, J. Global Changes in the Diurnal Cycle of Surface Ozone. *Atmos. Environ.* **2019**, *199*, 323–333. <https://doi.org/10.1016/j.atmosenv.2018.11.028>.
- (4) Orbe, C.; Oman, L. D.; Strahan, S. E.; Waugh, D. W.; Pawson, S.; Takacs, L. L.; Molod, A. M. Large-Scale Atmospheric Transport in GEOS Replay Simulations: TRANSPORT IN GEOS REPLAY SIMULATIONS. *J. Adv. Model. Earth Syst.* **2017**, *9* (7), 2545–2560. <https://doi.org/10.1002/2017MS001053>.
- (5) Larkin, A.; Geddes, J. A.; Martin, R. V.; Xiao, Q.; Liu, Y.; Marshall, J. D.; Brauer, M.; Hystad, P. Global Land Use Regression Model for Nitrogen Dioxide Air Pollution. *Environ. Sci. Technol.* **2017**, *51* (12), 6957–6964. <https://doi.org/10.1021/acs.est.7b01148>.
- (6) Gelaro, R.; McCarty, W.; Suárez, M. J.; Todling, R.; Molod, A.; Takacs, L.; Randles, C. A.; Darmenov, A.; Bosilovich, M. G.; Reichle, R.; Wargan, K.; Coy, L.; Cullather, R.; Draper, C.; Akella, S.; Buchard, V.; Conaty, A.; da Silva, A. M.; Gu, W.; Kim, G.-K.; Koster, R.; Lucchesi, R.; Merkova, D.; Nielsen, J. E.; Partyka, G.; Pawson, S.; Putman, W.; Rienecker, M.; Schubert, S. D.; Sienkiewicz, M.; Zhao, B. The Modern-Era Retrospective Analysis for Research and Applications, Version 2 (MERRA-2). *J. Clim.* **2017**, *30* (14), 5419–5454. <https://doi.org/10.1175/JCLI-D-16-0758.1>.
- (7) Environment and Climate Change Canada/Environnement et Changement climatique Canada. National Air Pollution Surveillance Program <https://open.canada.ca> (accessed May 11, 2021).
- (8) U.S. Environmental Protection Agency. Air Quality System Data Mart <https://www.epa.gov/airdata> (accessed Nov 24, 2020).
- (9) European Environment Agency. Air Quality e-Reporting Air quality annual statistics <https://www.eea.europa.eu/> (accessed May 11, 2021).
- (10) Lamsal, L. N.; Duncan, B. N.; Yoshida, Y.; Krotkov, N. A.; Pickering, K. E.; Streets, D. G.; Lu, Z. U.S. NO₂ Trends (2005–2013): EPA Air Quality System (AQS) Data versus Improved Observations from the Ozone Monitoring Instrument (OMI). *Atmos. Environ.* **2015**, *110*, 130–143. <https://doi.org/10.1016/j.atmosenv.2015.03.055>.
- (11) Martin, R. V.; Brauer, M.; van Donkelaar, A.; Shaddick, G.; Narain, U.; Dey, S. No One Knows Which City Has the Highest Concentration of Fine Particulate Matter. *Atmospheric Environ. X* **2019**, *3*, 100040. <https://doi.org/10.1016/j.aeaoa.2019.100040>.